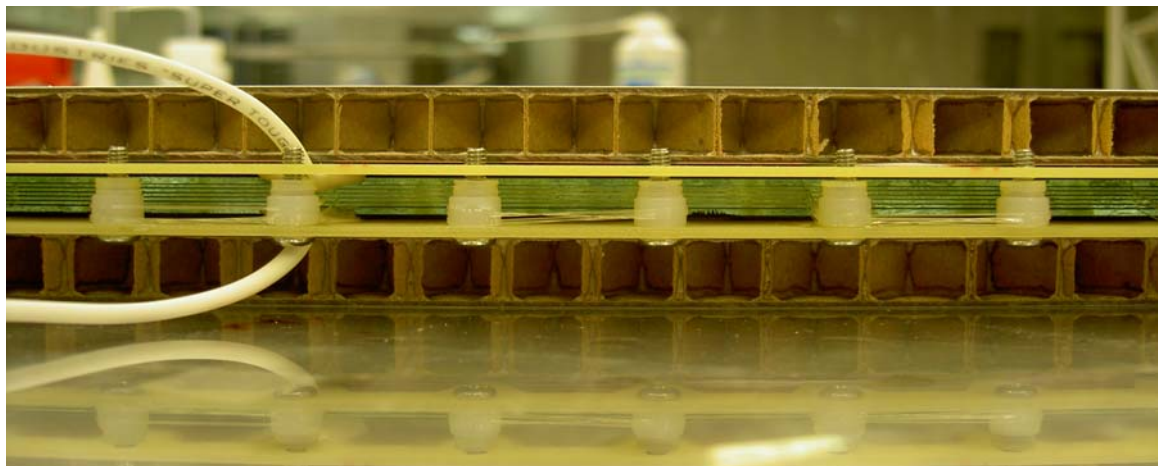# Multi-gap Resistive Plate Chambers: Time-of-Flight system of the PHENIX high-p$_T$ Detector

Conceptual Design Report

June, 2005

Multi-gap Resistive Plate Chambers: Time-of-Flight system of the PHENIX high-p$_T$ Detector

Tof – West team

J. Velkovska, T.Chujo, V.Greene, C. Maguire, H. Valle, D. Mukhopadhyay, D. Pal, I.Ojha, M. Velkovsky, M. Holmes, M. Mendenhall, J. Wallace, B. Love, R. Bekele, D. Ferrara, J. Fellenstein, T. Brasoveanu

Vanderbilt University

Y. Miake, S. Esumi, M. Inaba, S. Kato, S. Sakai, H. Masui, M. Konno, M. Shimomura, Y. Nagata, M. Oka, M. Narisawa, K. Miki, N. Sato, Y. Ikeda, R. Tanabe, Y. Tomita, T. Niita

Tsukuba University

E. O'Brien, D. Lynch, P. Kroon, A. Ruga, R. Ruggiero, S. Boose, R. Pisani, C. Biggs, J. Haggerty

Brookhaven National Laboratory

C.-Y. Chi
Nevis Laboratory

W.L. Llope, G. Eppley, T. Nussbaum

Rice University

L. Kotchenda
Moscow Enineering Physics Institute

Contents:

1. Overview

We propose to implement a cost - effective Time-of-Flight (TOF) detector for PHENIX, based on Multi-gap Resistive Plate chambers (MRPC). This detector will provide high-resolution timing measurement in the PHENIX West arm and together with the Aerogel Cerenkov Counters (ACC) will complete the planned high-p_T upgrade. The goal is to achieve timing resolution of ~ 100 ps, which will supplement the PID provided by ACC and the Ring Imaging Cerenkov Counter (RICH) and thus allow for continuous PID for pions, kaons and protons in the range $0.2 < p_T < 9$ GeV/c. The complete system will be in place by RUN6 of RHIC. The R&D efforts on this project have taken full advantage of previous worldwide R&D efforts, both in the detector construction and in the readout electronics. Within 1.5 years, we have developed several prototypes and undergone a beam test at KEK and in PHENIX during Run5. The detectors and electronics have been tested in real operating conditions. This document provides the conceptual design report for the full system that is proposed to be built and installed in PHENIX. The document is organized as follows: Section 2 provides the physics motivation for this project; Section 3 outlines the role of the high-resolution TOF detector within the high-p_T detector. Section 4 describes the R&D studies completed before Run 5 and the results from the beam test at KEK. Section 5 describes the detector and electronics R&D studies for RUN5 and the results obtained from the test in PHNIX. Section 6 contains the conceptual design for the full detector system. Section 7 outlines the proposed production procedures and quality assurance tests. Section 8 give a cost and schedule estimate.

2. Physics Motivation

We have witnessed exciting discoveries at RHIC. The suppression of high-p_T inclusive charged hadrons [1,2], π^0 [1,3] K_s [4] and the absorption of the away-side jets [5] are all consistent with "jet-quenching" as predicted [6] to appear with the presence of QGP. The measurements [7-10] in *d+Au* collisions showed beyond doubt that the observed effects in *Au+Au* collisions are due to the final state.

Figure 1 shows the PHENIX results obtained in sqrt(s) = 200 GeV *Au+Au* and *d+Au* collisions. The yields of neutral pions are measured in the two systems and compared to the yields obtained in p+p collisions (also measured by PHENIX [11]). The ratio of the yields in *Au+Au* collisions scaled appropriately to account for pure geometric factors and the yields in *p+p* collisions reveals a factor of ~5 suppression. The effect is not present in *d+Au* collisions. Initial state effects such as parton saturation [12] have been excluded as a possible explanation of the data
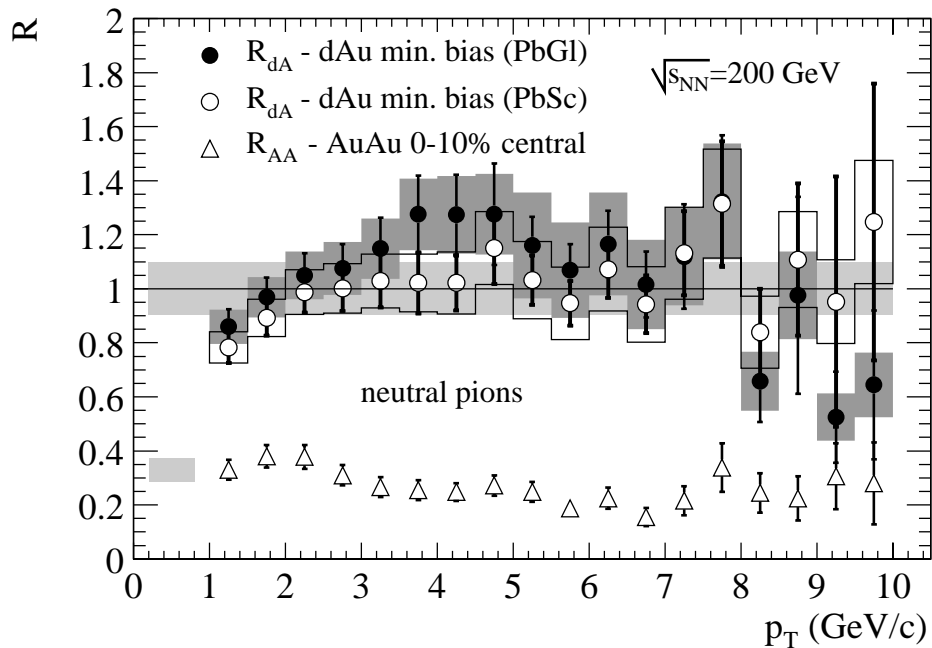

Figure 1. Nuclear modification factors for neutral pions produced in central Au+Au collisions or in d+Au collisions. A definitive test of "jet-quenching" has been provided.[7-10]

While hadron suppression was predicted by theory, the experimental results of proton and anti-proton production [13] have revealed completely unexpected features. In central *Au+Au* collisions at relatively high-p_T ($2 < p_T < 4$ GeV/c) protons and anti-protons constitute almost half of the charged hadron yield contrary to the known jet fragmentation functions. However, their production scales with the number of nucleon collisions as expected for particles produced in hard-scattering processes, but not affected by the nuclear environment.

Figure 2. shows the proton/pion and anti-proton/pion ratios in three different centrality classes: 0-10%, 20-30%, and 60-92% of the total inelastic cross section. The ratios depend strongly on centrality indicating that the dominant production mechanism of protons and pions is centrality dependent at high-p_T.
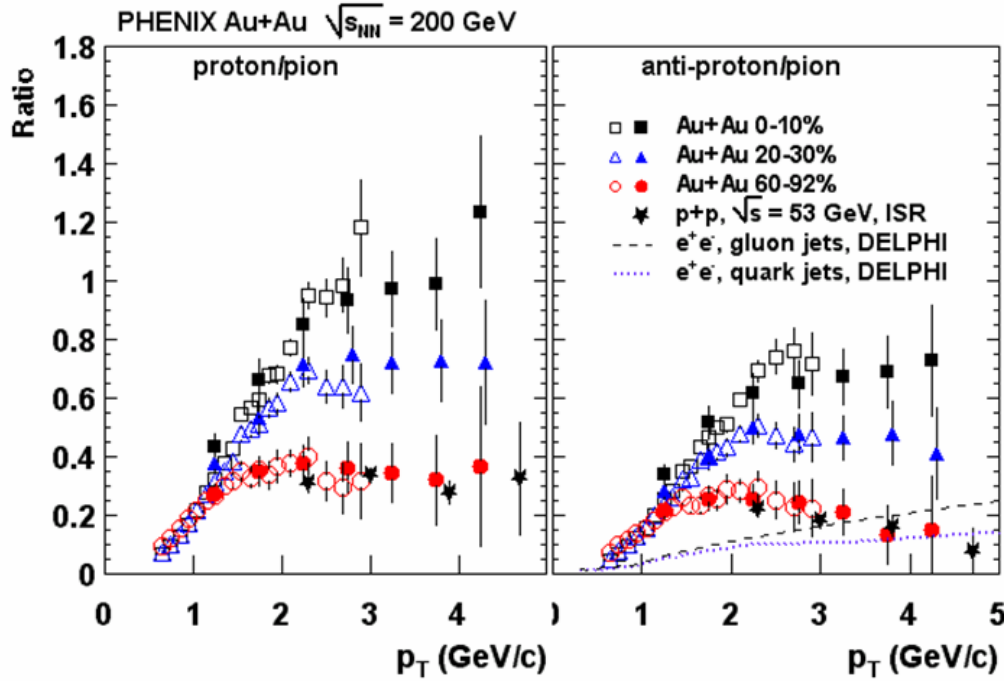

Figure 2: Proton/pion and anti-proton/pion ratios measured in Au+Au collisions at sqrt(s) = 200 GeV by PHENIX. Open (filled) points use charged or neutral pion data to form the ratio. For comparison, data obtained in lower energy p+p collisions and in e+e- collisions is also included.

The comparison with data obtained in lower energy p+p collisions and in e+e- collisions (included in the figure), shows that if both protons and pions are the products of hard-scattering, the fragmentation function in central *Au+Au* collisions must be rather different from that in peripheral collisions and in elementary systems. This result contradicts the common description of hard-scattering processes by a universal fragmentation function. An even bigger surprise is the result that the proton and anti-proton production is not suppressed at moderately high-pt. Figure 3. shows the comparison of the nuclear modification factors measured for pions, (proton+anti-proton)/2 and ϕ mesons. Above p_T = 2 GeV/c the measured baryon yield scales with N_{coll}, while meson production (π, ϕ) is suppressed.
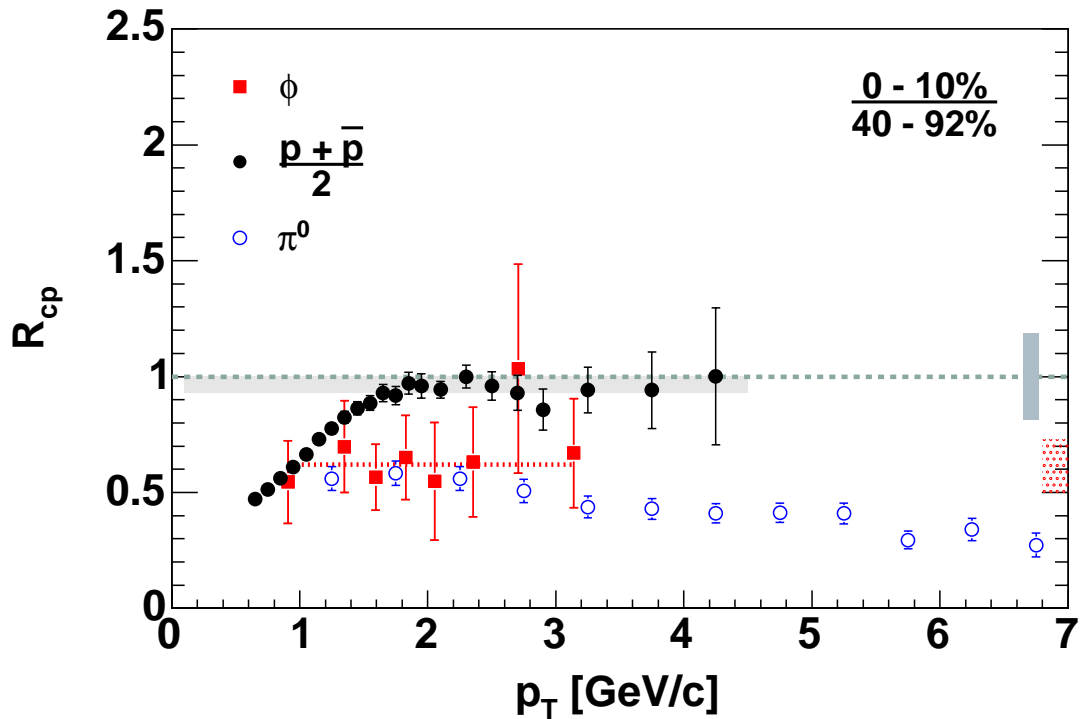
Figure 3: Nuclear modification factor for neutral pions, protons+anti-protons and φ mesons measured by the PHENIX experiment in sqrt(s) = 200 GeV.

Similar results have been obtained by the STAR experiment in the strange particle sector. Baryons and mesons show different behavior at moderately high-p_T. Only beyond p_T = 5 GeV/c, there is an indication that "normal" jet fragmentation returns. A number of exciting theoretical descriptions have attempted the explaination of the data. These include recombination of quarks from a thermalized system, the formation of an exotic gluonic configuration – the baryon junction or strong species dependent initial multiple scattering (Cronin effect). All of these theories call for significantly extended PID capabilities. This proposal aims at the development of a detector that will provide that.

Another observable that is sensitive to the early stages of the collisions and has brought most unexpected results in the identified particle sector is elliptic flow.

Elliptic flow at low-p_T is a collective effect. In the presence of bulk matter and strong pressure gradients, it transforms the initial anisotropy in position space (the ``almond'' of overlap between the nuclei) into momentum anisotropy. At high-$p_T$, azimuthal anisotropy can be generated by jet-quenching due to the different absorption along the short and long axes of the ``almond''. Elliptic flow is measured through the second Fourier component, v2, of the particle momentum

distributions with respect to the reaction plane. The maximum possible v2 at low-p_T is given by ideal (non-viscous) hydrodynamics. At high-p_T the limit is geometric and is maximal in the surface emission scenario, where partons traversing dense medium are completely absorbed due to large energy loss.

Hydrodynamics has been successful in describing low-p_T elliptic flow data both for inclusive and identified hadrons and the mass dependence v2 (pion) > v2(Kaon) > v2(proton). At high-p_T the large, p_T-independent v2 measured for charged hadrons exhausts or even exceeds the limit of surface emission [14]. The measurements of elliptic flow with identified particles have shown deviations from the hydrodynamics description with the heavier particles protons and Λ decoupling at slightly higher p_T than the lighter ones (pions and kaons). At high-p_T v2 saturates, with the baryons carrying the largest signal. If this azimuthal anisotropy is due to energy loss, then it should also be reflected in larger suppression in R_{cp} contrary to the results presented above. Another puzzle has emerged. Recombination models have been proposed to resolve it [15].

On the experimental part, the availability of broad momentum range PID detector has become a necessity. This motivated the development of the PHENIX high-p_T detector.

3. The PHENIX high-p_T detector

The PHENIX high-p_T proton and anti-proton results have posed many difficult questions to the theory. Measurements of identified hadrons with p_T well above 5 GeV/c have become absolutely necessary. In the baseline configuration, PHENIX is equipped with a high-resolution TOF detector with timing resolution ~100 ps which gives pion, kaon and proton identification to moderately high-p_T. In addition, a Ring Imaging Cerenkov Counter operating with CO_2 gas with index of refraction n=1.00041 at 1 atm, gives charged pion identification for p_T >5.5 GeV/c. A Cerenkov detector with index of refraction n = 1.01 can fill the gaps in PID that are left between the TOF and RICH. Such detector was designed and built as part of the PHENIX upgrade program.

The additional Cerenkov counter is based on aerogel, which is a silicon-based solid with a porous, sponge-like structure in which 99 percent of the volume is air. It is one of the least dense solids known. Aerogel has attracted much interest as a Cerenkov radiator because it is a solid but has index of refraction smaller that most liquids and solids (only liquid He is close), but larger than gasses at atmospheric pressure.

The PHENIX Aerogel Cerenkov Counter   consists of 160 elements of hydrophobic aerogel covering 1 sector, $\Delta \phi$ = 14° in azimuth and |$\Delta \eta$ | < 0.35, in the West arm of PHENIX (Figure 4). In combination with a high-resolution

TOF detector and the already existing RICH, PID can be achieved up to $p_T \sim$ 9 GeV/c for pions, kaons, protons and anti-protons. This will allow for a crucial test of quark-recombination and baryon junction models above $p_T = 5$ GeV/c.
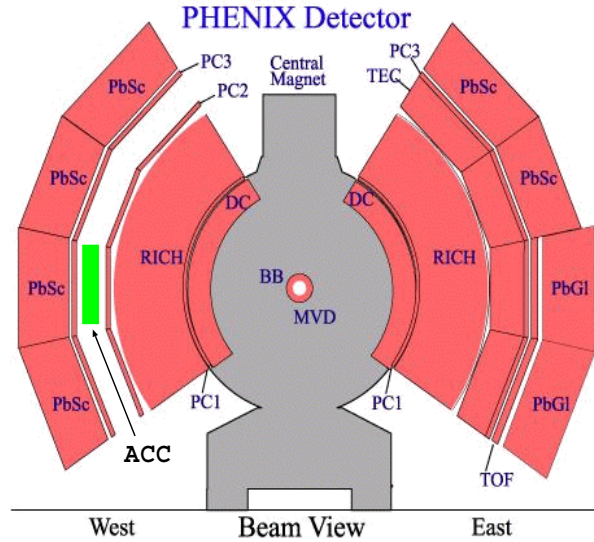

Figure 4. The Aerogel detector installed between Pad Chamber 2 (PC2) and 3 (PC3) in the W1 sector of the PHENIX West Central Arm.
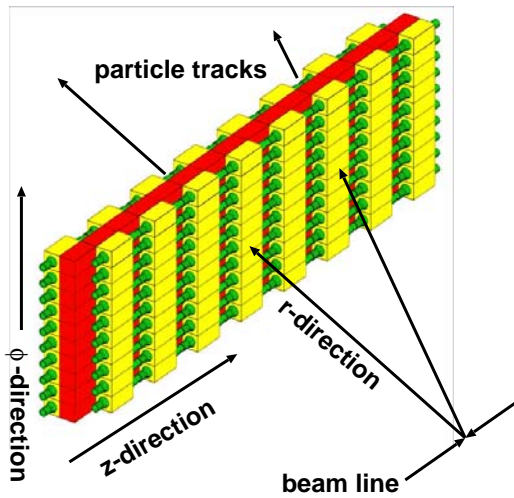

Figure 5. The Aerogel detector structure and the orientation with respect to the beam line are shown. The yellow boxes represent the aerogel volumes. The green tubes are the PMTs arranged to minimize dead areas. The red boxes represent the support structure.
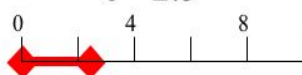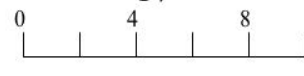
		Pion-Kaon separation	Kaon-Proton separation
TOF	σ~100 ps	0 - 2.5	- 5
RICH	n=1.00044 γth~34	5 - 17	17 -
Aerogel	n=1.01 γth~8.5	1 - 5	5 - 9

Figure 6. PID scheme using the combination of TOF, RICH and ACC. For each detector, the red lines indicate the region of transverse momentum in which particle separation is achieved.

Figure 6 illustrates the PID scheme using the combination of TOF, RICH and ACC with n=1.01. For each detector, the red lines indicate the region of transverse momentum in which particle separation is achieved. The TOF detector (with resolution σ ~100 ps) provides a 4 σ π/K and K/p separation up to p_T 2.5 and 4.5 GeV/c, respectively. The RICH detector gives pion identification above p_T 5.5 GeV/c. The ACC turns on for pions at p_T = 1 GeV/c and for kaons - at p_T = 5 GeV/c,thus filling the gap in π/K separation in the region 2.5 < p_T < 5 GeV/c, where neither RICH nor TOF can separate pions from kaons. ACC also provides K/p discrimination for p_T > 5 GeV/c, where TOF identification is no longer possible. We note that ACC as built uses n=1.011, which has somewhat lower turn-on momenta for kaons and protons than the originally proposed.

In Run4 and Run5 timing information for low-p_T PID was provided from the Pb-Scintillator electromagnetic calorimeter, which has timing resolution of σ ~ 450 ps. This is significantly worse than the required resolution needed to achieve seamless PID for π,K,p up to p_T = 9 GeV/c. In this configuration, pion identification is unaffected, but kaon and proton PID is significantly reduced. Kaons can not be identified in the region   2 < p_T < 5 GeV/c. A similar PID gap exists for protons. We note that this is the region where recombination is expected to dominate. It is clear that without a high-resolution TOF detector, the continuous PID coverage and many of the physics goals for the high-p_T detector are compromised.

We propose to build a high resolution TOF detector in the West arm of PHENIX. We have investigated Multi-gap Resistive Plate Chamber (MRPC) technology as a cost-effective solution for a large ares TOF detector.

4. MRPCs R&D studies

4. a Overview of MRPCs in ALICE and STAR.

MRPCs have been implemented successfully in the STAR detector [16] and are being built for the STAR large area TOF upgrade [17]. They are also being implemented by the ALICE experiment [18] at the Large Hadron Collider - CERN. A vast amount of costly and time-consuming R&D work has already been done in this direction by the ALICE and STAR collaborations. Our approach has been to build on existing technology and work in close collaboration with the STAR TOF group. We have done our own R&D studies which are aimed to match the PHENIX detector resolution, occupancy and electronics requirements. In this section, we give an overview of the worldwide MRPC studies. The PHENIX R&D results are discussed in Sections 4.b and 4.c .

Two types of MRPCs have been investigated in the course of the ALICE R&D development: single stack and double stack. A schematic view in the two cases is shown in Figure 7. In both cases, the detector consists of a stack of resistive plates (float glass), spaced from one another with equal sized spacers creating a series of gas gaps. Monofilament fishing line is used as spacers. Electrodes (carbon tape) are connected to the outer surfaces of the stack of resistive plates, while the internal plates are left electrically floating. The signals are imaged on copper pick-up pads. In the double stack design, two MRPCs are built on each side of the anode pick-up pads. The advantages in this configuration are larger signals, reduction in the required HV, anode and cathode can be moved closer which makes the footprint of the avalanche smaller and thus sharpens the pad boundaries. In the final design, ALICE uses 10 gap double stack MRPCs. The chambers have active area of $7x120 \text{ cm}^2$ and are readout by pads with area $3.5x2.5 \text{ cm}^2$.

From the point of view of performance, the single stack design is comparable to the double stack design as illustrated in Figure 8 and Figure 9.
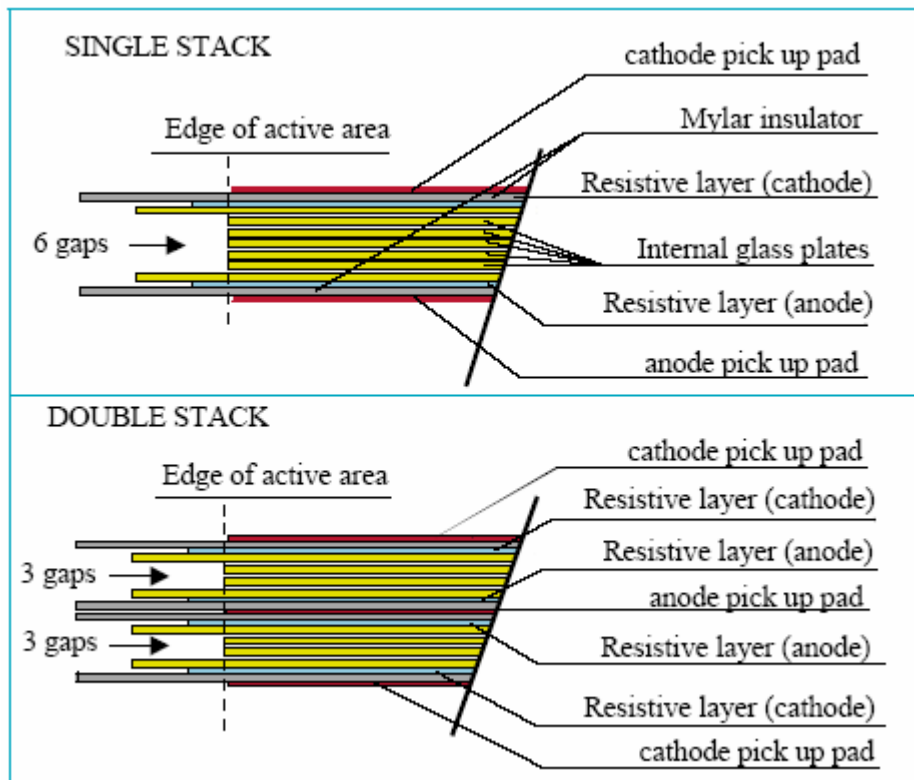
Figure 7. MRPC designs investigated for ALICE (figure taken from ref. [18]).

A single stack 6 gap configuration was chosen for STAR with outer glass thickness 1.1cm, inner glass – 0.55cm and gap size – 220 μm. This design is simpler than the double stack and although it has slightly worse resolution and efficiency, the STAR collaboration has found that the performance is satisfactory. The pick-up pads have dimensions 3.15cm x 6 cm. The chambers have active area 20 cm x 6 cm. The read-out is single ended. The PCB layout with the six read-out pads is shown in Figure 10. Full 2π azymuthal coverage at a radial distance of 2 m is envisioned and currently under construction. Figure 11 shows the typical performance plot for the STAR MRPCs. The resolution quoted is obtained after slewing corrections and subtraction (in quadrature) of the start time resolution, which is measured independently. These results were obtained with gas mixture 90%/5%/5% $C_2H_2F_4$ (Freon R134a), i-C_4H_{10}, SF_6. The SF_6 is used to quench streamers and allows safe operation at voltages > 15 kV.
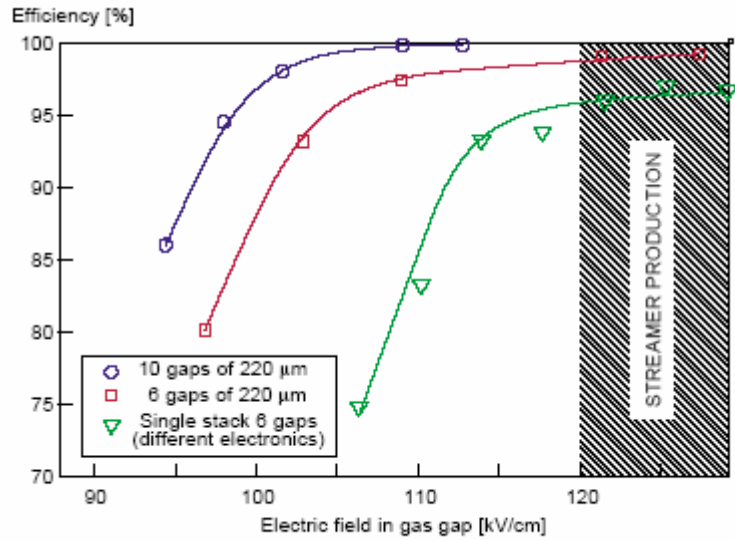
Figure 8. Efficiency as a function of electric field strength for double stack (10 gaps) and single stack (6 gaps) MRPC tested by ALICE group [ref.18.].
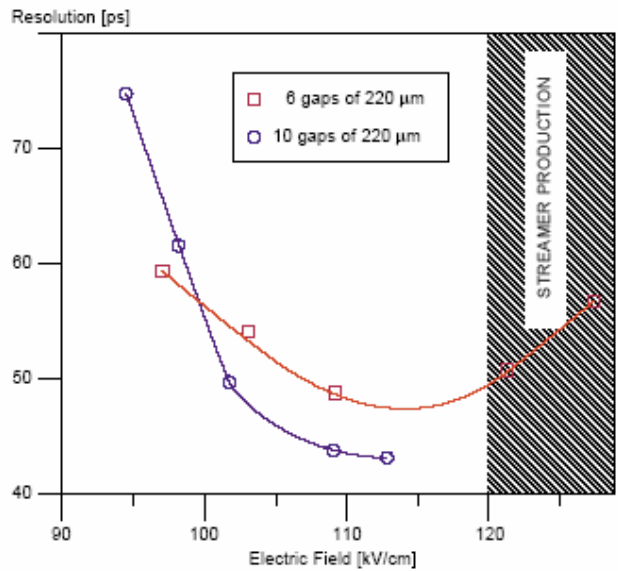
Figure 9. Comparison of timing resolution of single stack and double stack MRPC researched fro ALICE (figure from ref.[18]).
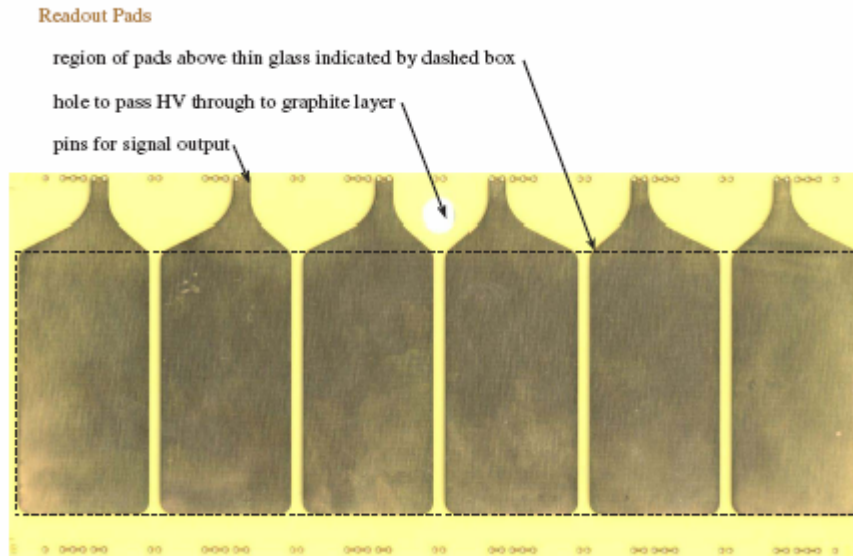
Figure 10. Read-out configuration (PCB) of the STAR MRPC detectors (from ref.[18]).The active area (dashed line) is 20 cm x 6 cm; pad size - 3.15 cm x 6 cm; pad spacing - 3 mm.
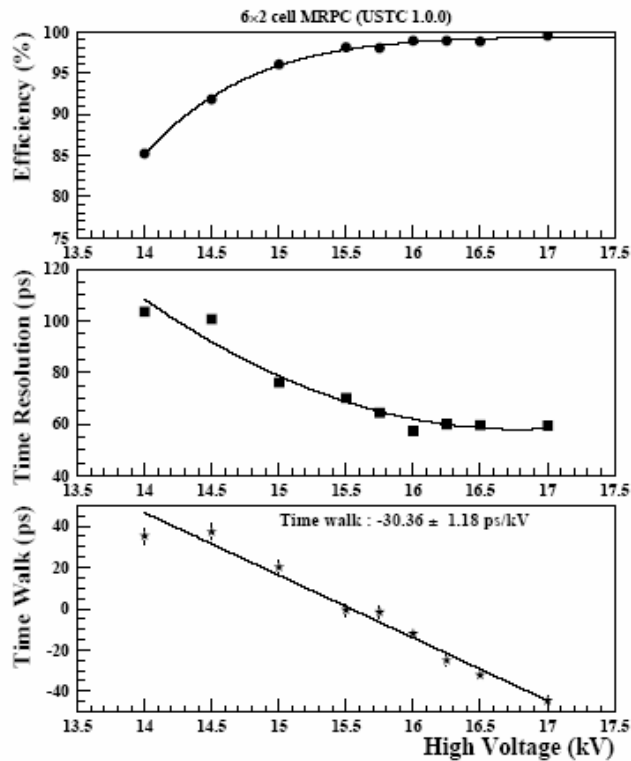
Figure 11. The detection efficiency (upper frame), slewing-corrected time resolution (middle frame), and time walk (lower frame), as a function of high voltage for the 6 gap MRPC implemented for the STAR upgrade. (the figure is from ref. [17]). These results were obtained with gas mixture 90%/5%/5% $C_2H_2F_4$ (Freon R134a), i-C_4H_{10}, SF_6. The SF_6 is used to quench streamers and allows safe operation at voltages > 15 kV.

### 4. b Considerations for PHENIX. Prototype designs. KEK test.

Several factors have played a role in designing the PHENIX MRPC prototypes. The aggressive schedule has certainly biased us towards simpler solutions. The success of the STAR MRPC detector tests has influenced our decision to implement a single stack design with 6 gaps. Below we describe all other design parameters that are important for the performance and justify our choice for the PHENIX prototypes.

Thickness of inner and outer glass:

The thickness of the glass together with the gap sizes determines the electric field strength in the gaps. We followed the STAR design in choosing this parameter: 0.55mm for the inner glass and 1.1mm for the outer glass. This choice was also bound to the sizes that were available from Precision Glass and Optics.

Gap size:

The sensitivity to the gap size is not significant. The bigger gap sizes reduce the electric field strength (for the same voltage applied), but at the same time the avalanches are allowed to grow longer – hence the overall gain is not affected. Figure 12 demonstrates the performance of 6 gap MRPCs tested for ALICE using different gap sizes. Varying the gap from 280 μm to 220 μm does not influence the performance in the voltage plateau region. We have chosen 230 μm gaps. Monofilament fishing line is used for spacers.
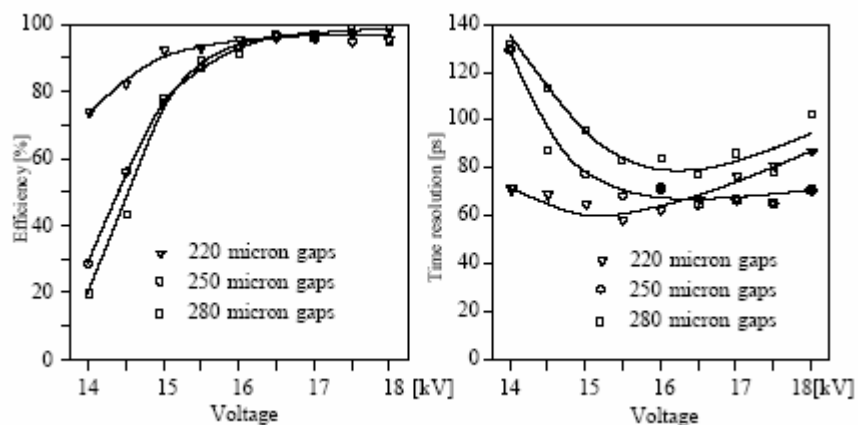
Figure 12. ALICE R&D plot from [17] shows the efficiency and resolution as a function of HV for single stack 6 gap MRPCs with different gap sizes.

Gas mixture:

The gas mixture used by ALICE is 90%/5%/5% $C_2H_2F_4$ (Freon R134a), i-C_4H_{10}, SF_6. Since SF_6 is a ODH (oxygen deficiency hazard) gas, the STAR detectors use a two component mixture: 95%/5% $C_2H_2F_4$ (Freon R134a), i-C_4H_{10}. The SF_6 gas is important for the performance, since it quenches the streamers and allows streamer-free operation at higher voltages and thus improves the efficiency and the resolution of the MRPC. With the two-component mixture, the resolution is 80-100 ps and the typical efficiency is of the order of 95%. This is to be compared to 60ps and >95% efficiency shown in Figure 11, where a 3-component gas mixture was used.

Chamber size:

Our original intent was to cover the active area behind the aerogel detector in the W1 sector, which is 4m x 1.20 m. This is less than the active area of the pad chambers PC2 and PC3. The goal was to minimize the number of readout channels and MPPC chambers. In this case, it is desirable to work with larger chambers and arrange them in two rows along the y-direction. We tried to build the biggest chambers that could fit in the space available and use the regular stock sizes of the glass sheets supplied by Precision Glass and Optics.

The inner glass (0.55 mm thickness) is available in sheets 20" x 20". Our prototype PH1 was designed as a square chamber using the above glass size. As shown above, the ALICE and the STAR MRPCs have very different dimensions. STAR uses really small chambers (inner glass $20x6$ cm^2). ALICE has long and narrow chambers: 120×7 cm^2. Coming up with squares: 53.3×53.3 cm^2 seemed like a big departure from the already researched designs. Concerns about being able to control the uniformity of the gas gaps and HV lead to making prototype chamber that is ¼ size of PH1. We built 2 different ¼ size prototypes: PH2 and PH3 that have the same glass dimensions, but different readout configuration.

Readout pads/strips:

The idea is to use a configuration which is as close as possible to TOF East, so that we have similar occupancy and readout configuration. Strips with double ended readout were implemented for PH1 and PH2. The layout of the strips used in for PH1 is shown in Figure 13. The timing information is obtained using the average time measured at both ends of the strip. The position information along the strip is determined using the measured time difference. Figure 14 shows the readout configuration for PH2 and PH3. Since both STAR and ALICE use 3 mm gaps between pads to prevent cross talk, we made our strips 1.3 mm wide with 3 mm separation gap between them. The length of the active area is determined by the size of the inner glass (53.3 mm). These sizes are to be compared to the area of the TOF

slats : 1.5x64 cm^2 and 1.5 x 42 cm^2. Hence, for PH1 and PH2 we expect occupancy <10% in central *Au+Au*. The number of strips was also chosen so that we have readout channels in multiples of 16 in order to match the segmentation of the TOF FEMs. PH1 has 32 strips (4 FEM modules), while PH2 has 8 strips (1 FEM module).
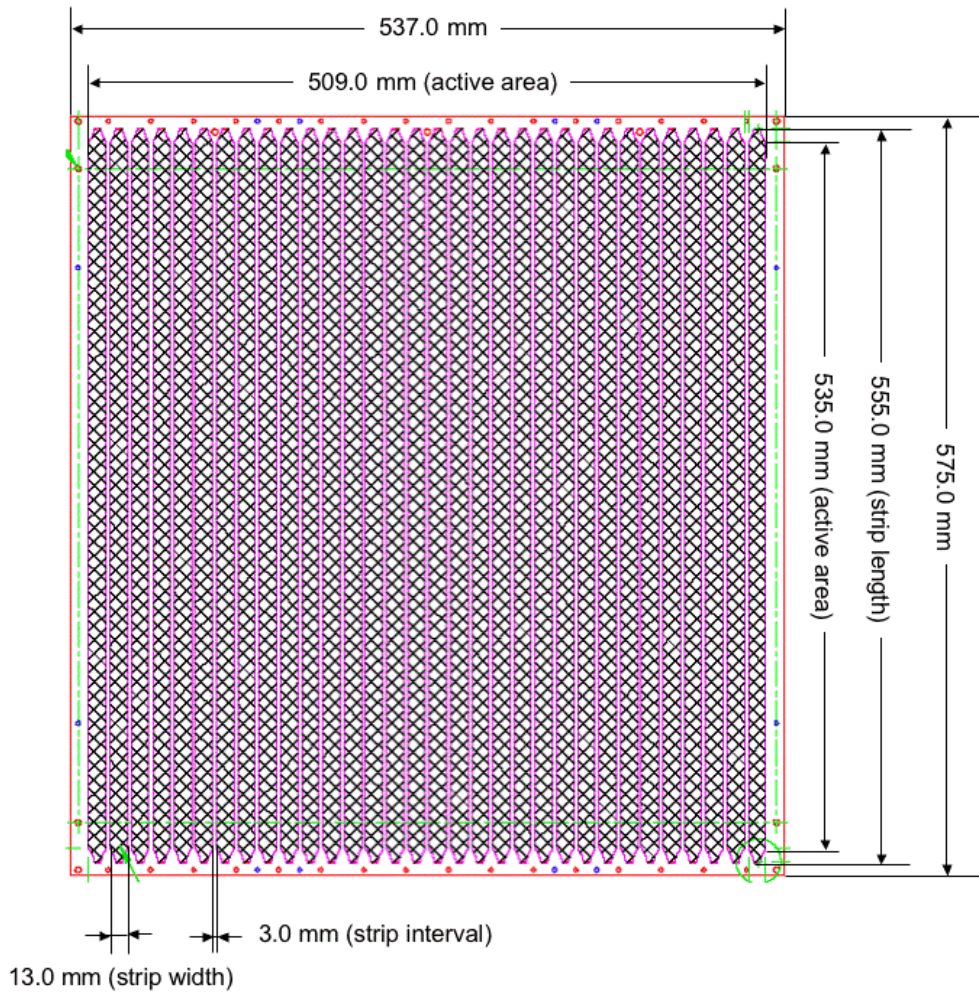
Figure 13. Pick-up PCB configuration in PHENIX prototype 1 (PH1). 32 strips are read out from both ends to determine the time and position of the charged avalanches produced by particles traversing the detector.
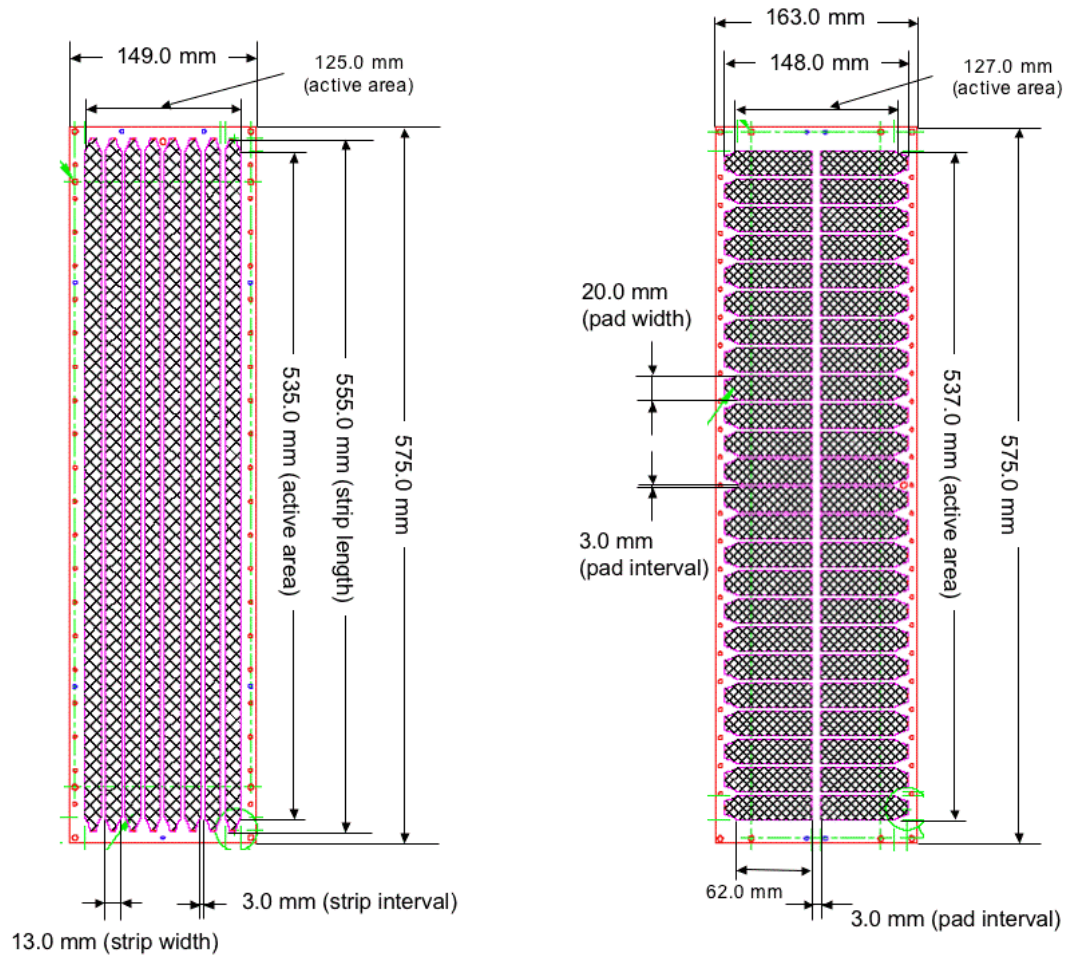
Figure 14. Pick-up PCB layout for PHENIX prototypes 2 and 3. PH2 is shown on the left and PH3 is on the right. PH2 is ¼ of the size of PH1. PH3 has the same dimensions as PH2, but is read out by pads.

Since neither STAR nor ALICE has implemented strip readout, and there was a concern that large capacitance in the strips will ruin the good timing resolution, we decided to make one prototype that follows more closely their design. We wanted to keep the other parameters the same as for PH2, but to make a single ended read out using pads. Keeping the number of channels in multiples of 16 was another factor that played in choosing the number of pads in PH3. As shown in Figure 14, PH3 has 48 readout pads with dimensions 2 x 6.2 cm^2. This configuration, of course, increases the number of electronics channels by a factor of 3, which is a significant part of the cost of the whole system. It was desirable, in case of similar performance, to use PH2 instead of PH3.

The cross sectional view for the PHENIX MRPC (PH2) is shown in Figure 15. The sizes of all components are shown in the figure.
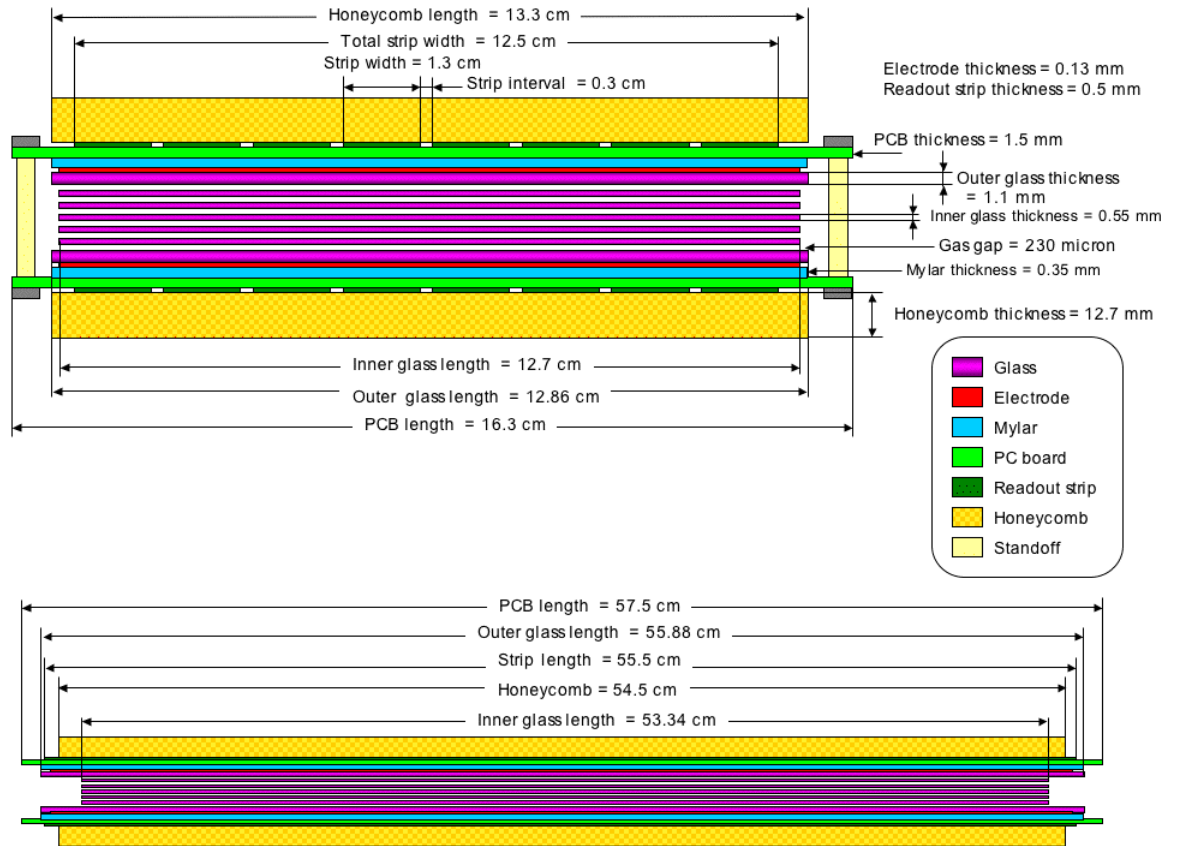
Figure 15. Cross sectional view showing all component sizes for the PH2 design.

The three MRPC prototypes were tested at KEK (High Energy Accelerator Research Organization), in Tsukuba, Japan in June 2004. We used secondary beams produced by the internal target in 12 GeV Proton Synchrotron. The beams were extracted to the experimental area, called T1 beam line. Positively charged particles with momentum of 2 GeV/c were used for this test. The beam consisted mainly of pions and protons (about 50%/50%). A small amount of deuterons and kaons were also identified.

A schematic view of the experimental setup is shown in Figure 16. Figure 17 shows a photograph of the setup with the different elements labeled in the picture. Three plastic scintillation counters (ST1, ST2, and ST3) which were read out by the photo-multiplier tubes at the both ends were used to obtain the start time information. The combination of 3 counters also allows the independent measurement of the resolution of the start time signal.The dimension of scintillation counter is 5x5 cm2 for ST1, and 2x2 cm2 for ST2 and ST3. Each counter has an intrinsic timing resolution of about 50 psec. Two defining counters, (DEF1 and DEF2, 1x1 cm2 each) were used to define the beam position. A VETO counter was used to reject background. The VETO counter was a large area scintillation counter (10x20 cm^2) that had a 1 cm diameter hole in the center. The hole was aligned with the defining counters. The beam trigger was determined by requiring a coincidence of ST1&ST2&ST3&DEF1&DEF2 and anti-coincidence with the VETO. The trigger rate was about 20 counts per beam spill, and the duration of spill is 2 sec. The MRPC was located 3 m away from the first start timing counter (ST1). Figures 16 and 17 also show a Time Projection Chamber (TPC) and an Electromagnetic Calorimeter (EMC) located downstream from the MRPC. These were part of a test performed by the Tsukuba group and were not used in this analysis.

The signals from the MRPC were pre-amplified and discriminated on boards that were positioned directly on the gas box. These are visible in Figure 17. The pre-amp boards were borrowed from Bill Llope from Rice University . These were originally used in the STAR test set-up. The signal from the pads is amplified by Maxim 3760 fast current amplifier, then amplified in a second stage to produce output into 50 Ω. The discriminator is based on the AD96685 comparator. The outputs from the amplifier and discriminator were connected to CAMAC ADC and TDC modules, respectively. The TDCs had 25 ps/channel and were operated in a COMMON START mode. The COMMON START signal was provided from the trigger signal described above. The individual MRPC strip or pad signals were used as STOP signals for the TDC channels.

KEK-T561 Experimental Setup

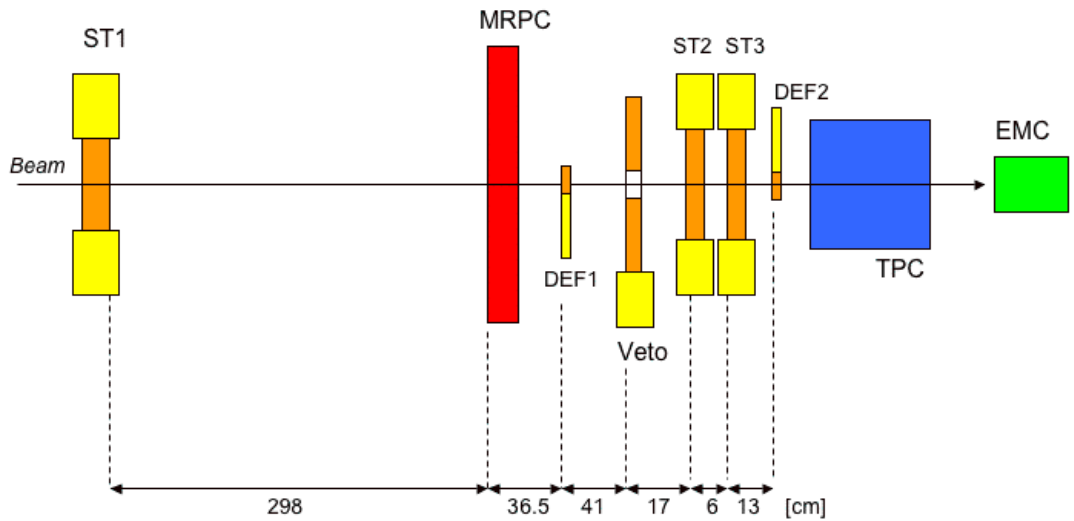Figure 16. A schematic view of the experimental set-up used for the beam test of the MRPC prototypes. Scintillator counters ST1, ST2 and ST3 are used to provide start timing information. DEF1, DEF2 are small-area scintillator counters used to define the beam position. Veto counter is used for background rejection
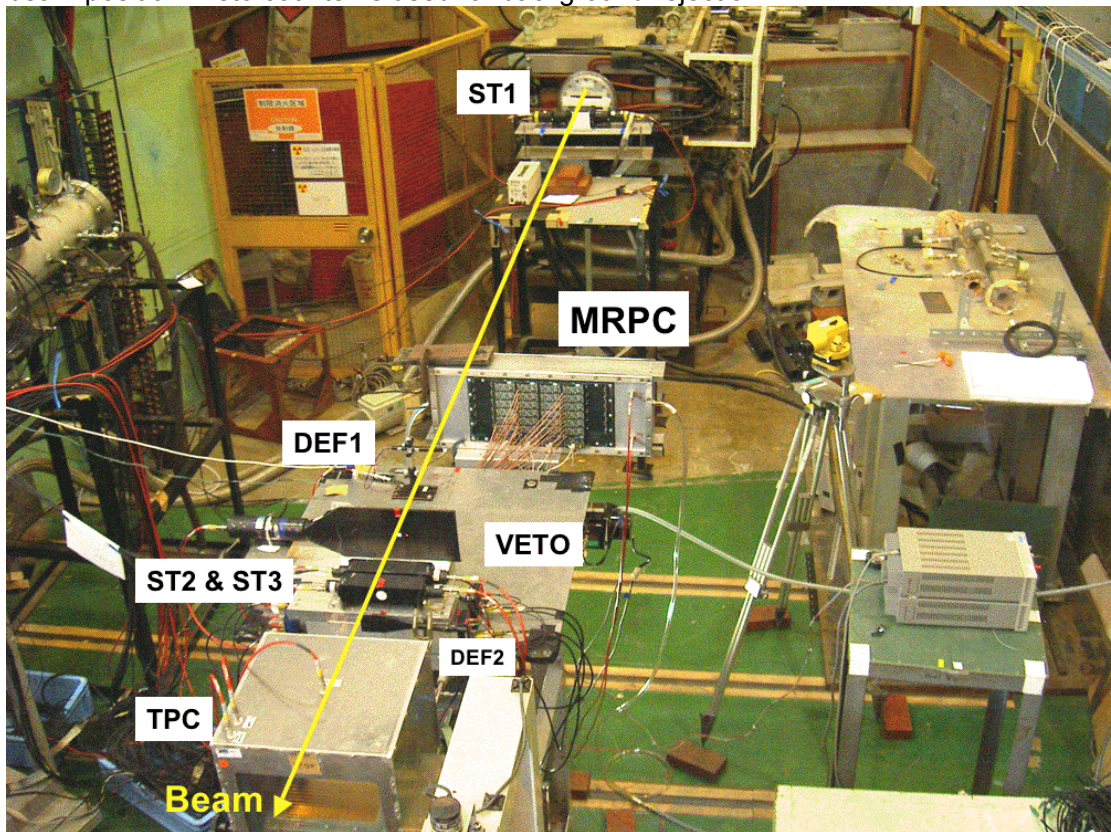

Figure 17. A photograph of the experimental set-up. The components for the test are labeled.

The following measurements were performed and the results were evaluated by comparing the timing resolution and the efficiency under the different conditions:

- Voltage scans
- Horizontal and vertical position scans
  – Across chamber
  – Within a pad
- Discriminator threshold scan (best results were obtained with the lowest threshold)
- Gas mixture (nominal: R134a/C4H10 95%/5%, 1cc/sec
  – 97%/3% (+/- 0.5%)
  – 92%/8% (+/- 0.5%)
  – Flow rate x 2
- Charge distribution (cross-talk)
- Streamer rate study (normally operate in avalanche mode)
- Electronics test – (use on-board discriminator or discriminate the analog signal as coming from the pre-amp boards.)

Figures 18,19, and 20 show performance plots for PH1,PH2 and PH3, respectively. These plots were obtained from the runs used in the voltage scans that are summarized in Figures 21 and 22. Plots for all runs are available at:

http://www.hep.vanderbilt.edu/~chujo/MRPC/KEK_ana/04.0701/fig/

The top left plots in the performance figures (Fig 18,19,20) show the TDC distribution of the average time obtained by ST2&ST3 with the time of ST1 subtracted. Two main peaks are visible: pions on the left and protons on the right. The small shoulder at the high end of the pion peak is due to kaons admixed with the main beam particles. A small deuteron peak is also present. The analysis was carried on with identified particles, since we wanted to know if the detector has uniform response to different particle species. The PID selection was done based on the top left plot. The top middle and top right plots show the timing distribution obtained from the MRPC using either ST1 or ST2&ST3 as a start time signal. Using the information from all three top plots, the intrinsic timing resolution of ST1, ST2&ST3 and the MRPC can be extracted separately. The MRPC results shown in the top plots are corrected for slewing. The slewing effect and the functions used for the correction are shown in the two bottom plots. There are two distinct peaks in the ADC distributions. The lower one is produced in avalanche mode, which is the normal operational mode of the MRPC. The top one is due to streamers, the percentage of which increases with the increase of the high voltage. The streamers have worse resolution (about 100 ps) and a larger charge footprint. Studies of hits in neighboring pads (done with PH3 when the beam is positioned in the center of the pad) show that in almost 100% of the cases these hit occur when the main pad develops a streamer. In the case of PH1 and PH2, we found that the strips are not wide enough to contain the charge footprint and hits were registered on the side strips even if no streamers were produced. The plots contain information about the HV setting, the channel in

which the main hit occurred, the discriminator threshold setting, the PID of the particle for which the numbers were derived, the efficiency, the intrinsic timing resolution of the MRPC and the start counters, the ADC fit range that was used to determine the slewing corrections, the percentage of hits that were due to streamers, the timing resolution of the MRPC (using ST1 as a start timer) after the slewing correction, but before subtraction the resolution of the start counter; the same quantity in the case of streamers.

Figures 21 and 22 summarize the timing resolution and efficiency results obtained from the voltage scan of the three prototypes. The two small chambers PH2 and PH3 show excellent timing resolution. We are particularly pleased that with the strip design (PH2) we achieved $\sigma \sim 70$ ps. These results are comparable to the results obtained by STAR with much smaller chambers and using pad readout (see Figure 11). The results from our pad design (PH3) are slightly worse concerning the timing resolution in this voltage scan. We have however observed that overall (from all runs with varying conditions), the performance of the pad design was a bit better. We must, however, take into account that in the case of the strip design, we can determine the position of the hit using the timing measurements alone. In the case of the pads, the test beam was well defined (within 1 cm^2) due to the defining counters. On carriage, we can not define the hit position with such accuracy, even if we use information from the tracking detectors. As a result, the timing measurement will be subject to smearing due to the spread in hit positions. Compared to PH2 and PH3, the resolution of the large chamber (PH1) was poor and to a large extent non-uniform across the detector. It is also apparent in Figure 17 that the gain in the particular channel shown in the figure is smaller than for the gain in PH2 and PH3. We attribute these observations to non-uniformities in the gas gaps that were very difficult to control in the big square chambers due to the larger weight of the glass and the lack of binding in the layers of glass and PCBs in the middle of the detector. It may be in principle possible using engineering analysis to make a better design for a square chamber in which the gas gaps are under control. However due to lack of R&D time, we decided to abandon this design and continue the development with the ¼ size chambers.

The pad design (PH3) showed excellent detection efficiency (Fig. 22) $\varepsilon = 95\%$. The efficiency for both strip designs is $\sim 90\%$. This value is lower than what we would like to have in our final implementation and we need to understand why the efficiency in bith PH1 and PH2 is smaller than for PH3. One obvious difference in the designs is the width of the pads/strips. The smaller side of the pads is 2 cm wide, while the strips are only 1.3 cm wide.We notice that both STAR and ALICE use pads that are wider (3 x 6 cm^2 and 2.5 x 3.5 cm^2).

Time3[MRPC]-Time2[ST2&ST3] (w/ slewing) 23_tdc_cor

Entries	6103
χ^2 / ndf	267.1 / 36
Constant	311.1 ± 6.296
Mean	-1.675 ± 0.09915
Sigma	6.443 ± 0.09567

TDC [ch]

hist23_ta Entries 6629

ADC [ch]

MRPC_ADC : Time3[MRPC]-Time2[ST2&ST3]

TDC [ch]

Time3[MRPC]-Time1[ST1] (w/ slewing) 13_tdc_cor

Entries	6103
χ^2 / ndf	276.2 / 37
Constant	310.9 ± 6.296
Mean	264.8 ± 0.09928
Sigma	6.447 ± 0.09544

TDC [ch]

hist13_ta Entries 6629

ADC [ch]

MRPC_ADC : Time3[MRPC]-Time1[ST1]

TDC [ch]

Time2[ST2&ST3]-Time1[ST1] _st12_tdc

Entries	6629
χ^2 / ndf	503.2 / 37
Constant	842.4 ± 13.92
Mean	-287.2 ± 0.03921
Sigma	2.901 ± 0.03042

TDC [ch]

Run #: 335

PH1, HV = 15.50 kV
threshold: 100 mV, hit ch. #: 2-3
PID: π^+ (p = +2.0 GeV/c)

ϵ (hit) : 92.07 [%]
ϵ (w/ next hit): 92.03 [%]
ϵ (all channel): 92.03 [%]

σ_T (MRPC) = 152.74 ± 0.38 ps
σ_T (ST1) = 51.45 ± 0.26 ps
σ_T (ST2&ST3)= 51.12 ± 0.27 ps
ADC fit range: 110 - 180 ch
Streamer: 7.42 [%] (453/6103)
σ_{13}(w/slewing) = 164.96 ps
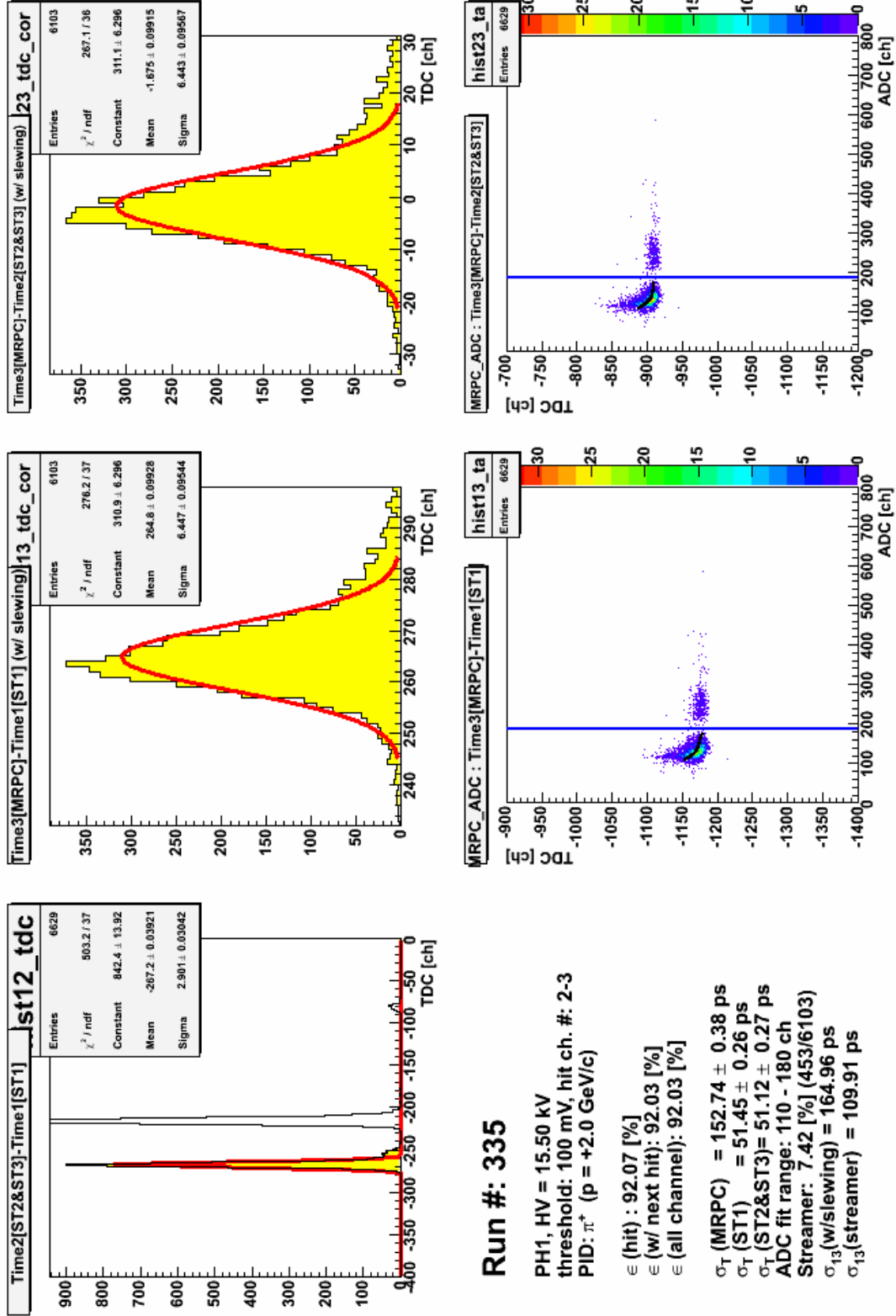σ_{13}(streamer) = 109.91 ps

Figure 18. Performance plot for PH1. The plots in the different panels are explained in the text.
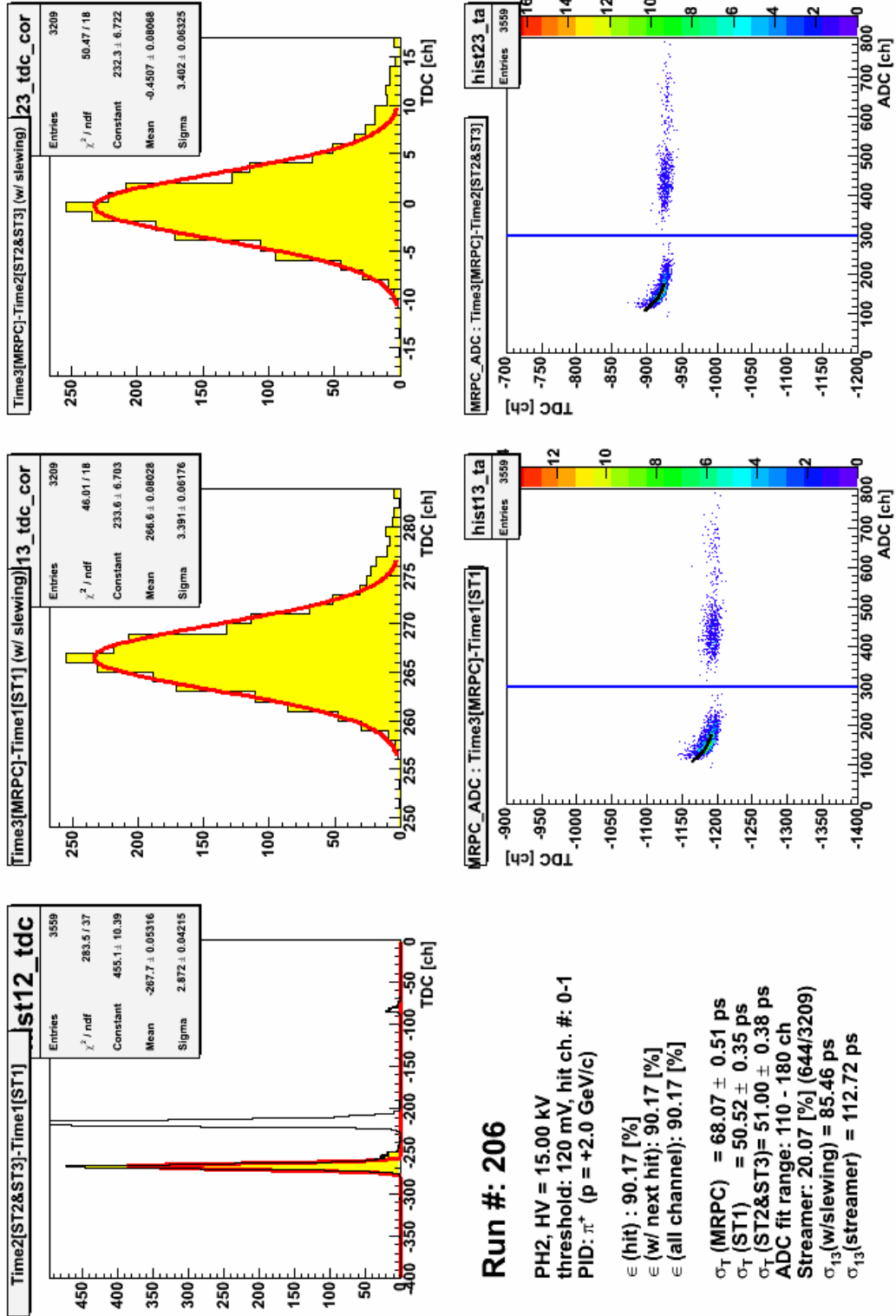
Figure 19. Performance plot for PH2. The plots in the different panels are explained in the tex.t

Time3[MRPC]-Time2[ST2&ST3] (w/ slewing) 23_tdc_cor

Entries	3620
χ^2 / ndf	61.67 / 23
Constant	306.1 ± 7.168
Mean	-0.2473 ± 0.07539
Sigma	4.25 ± 0.06751

TDC [ch]

Time3[MRPC]-Time1[ST1] (w/ slewing) 13_tdc_cor

Entries	3620
χ^2 / ndf	57.91 / 23
Constant	304.1 ± 7.136
Mean	267.1 ± 0.07608
Sigma	4.294 ± 0.06879

TDC [ch]

Time2[ST2&ST3]-Time1[ST1] _st12_tdc

Entries	3723
χ^2 / ndf	282.5 / 32
Constant	466.4 ± 10.53
Mean	-286.1 ± 0.05329
Sigma	2.944 ± 0.0437

TDC [ch]

hist23_ta   Entries 3723

MRPC_ADC : Time3[MRPC]-Time2[ST2&ST3]

TDC [ch]   ADC [ch]

hist13_ta   Entries 3723

MRPC_ADC : Time3[MRPC]-Time1[ST1]

TDC [ch]   ADC [ch]

Run #: 251

PH3, HV = 15.00 kV
threshold: 100 mV, hit ch. #: 11
PID: π^+ (p = +2.0 GeV/c)

ϵ (hit) : 97.23 [%]
ϵ (w/ next hit): 97.21 [%]
ϵ (all channel): 97.21 [%]

σ_T (MRPC)   = 93.26 ± 0.41 ps
σ_T (ST1)   = 53.15 ± 0.38 ps
σ_T (ST2&ST3) = 50.91 ± 0.36 ps
ADC fit range: 120 - 220 ch
Streamer: 4.92 [%] (178/3620)
σ_{13}(w/slewing) = 109.50 ps
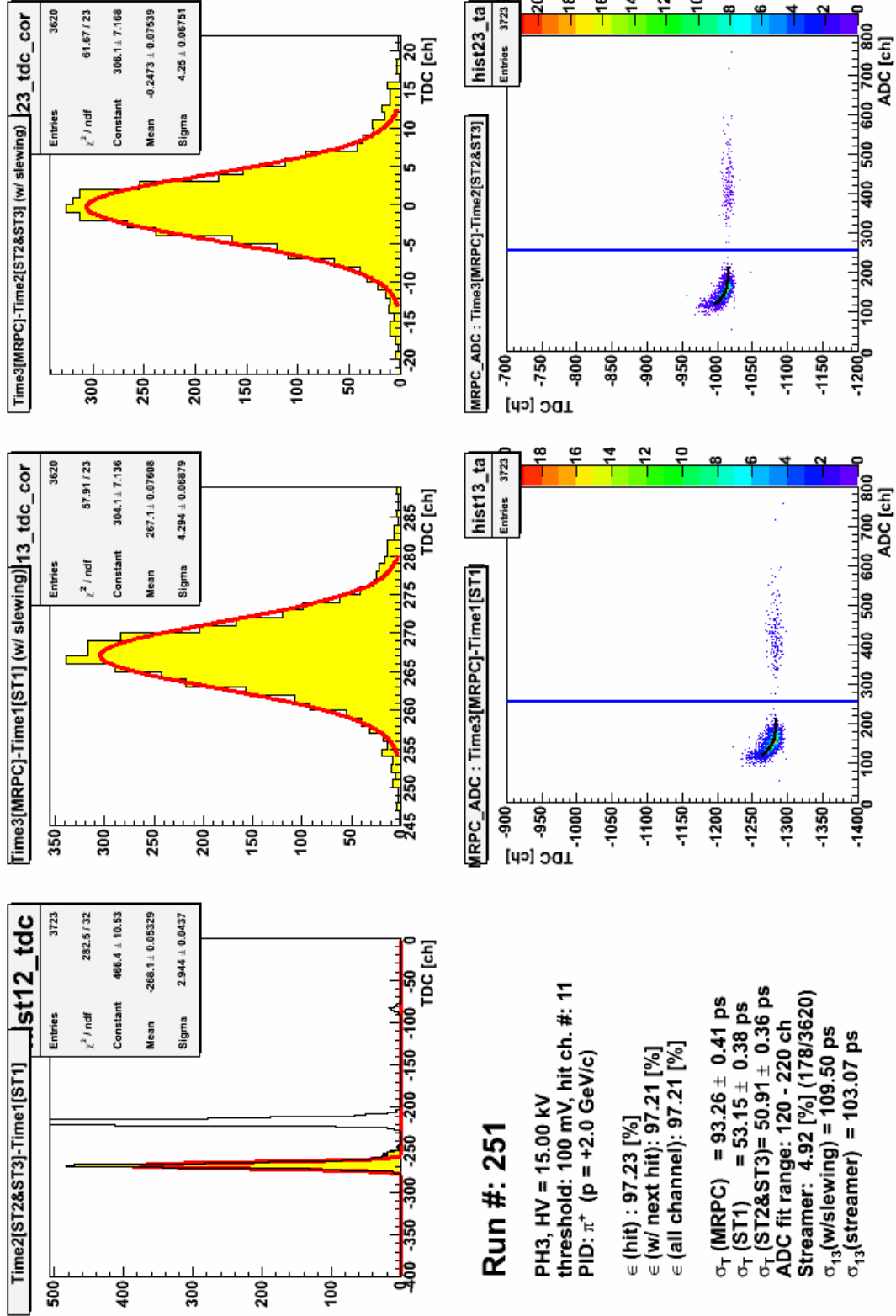σ_{13}(streamer) = 103.07 ps

Figure 20. Performance plot for PH3. The plots in the different panels are explained in the text.
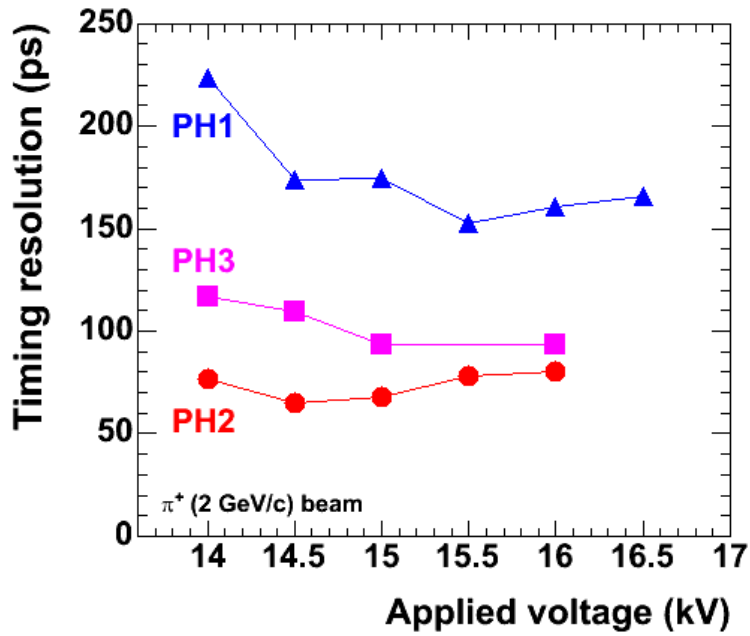
Figure 21. Timing resolution for the three prototypes as a function of the applied high voltage
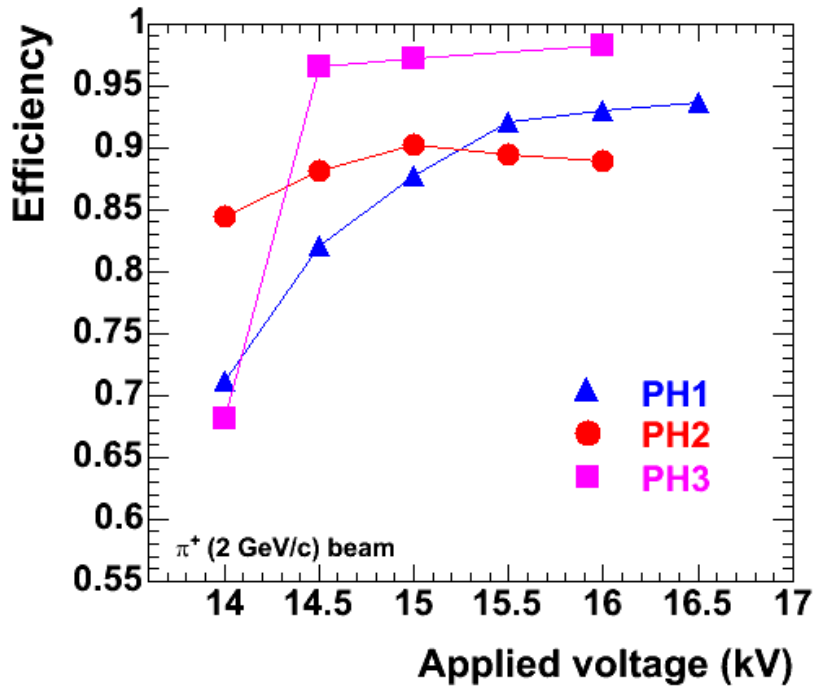

Figure 22. Efficiency for the three prototypes as a function of the applied high voltage

We performed horizontal and vertical scans along and across the strips/pads in order to study boundary effects. Uniform response was found along the strips of PH2. However across the width of the strips this was not the case. The efficiency varies depending on the position We found that the charge footprint is ~ 2.5 cm in diameter and that our choice of 1.3 cm wide strips is probably the cause of the reduced efficiency in PH1 and PH2. Since the charge gets split between two strips, it sometimes remains under the discriminator threshold and does not produce a hit. Figure 23 shows the horizontal scan across the pads of PH3. The efficiency registered in each pad is used as a measure for the extent of the charge distribution. The three pads are shown in different colors. The x-axis is shows the position of the hit (in cm). The efficiency across the pads has a nice high-efficiency plateau and then drops at the boundaries (but it may also fire the neighboring strip, so the hit is not completely lost). In the case of streamers, though, double hits do occur even if the beam is positioned at the middle of the strip. This is due to the wider charge footprint.
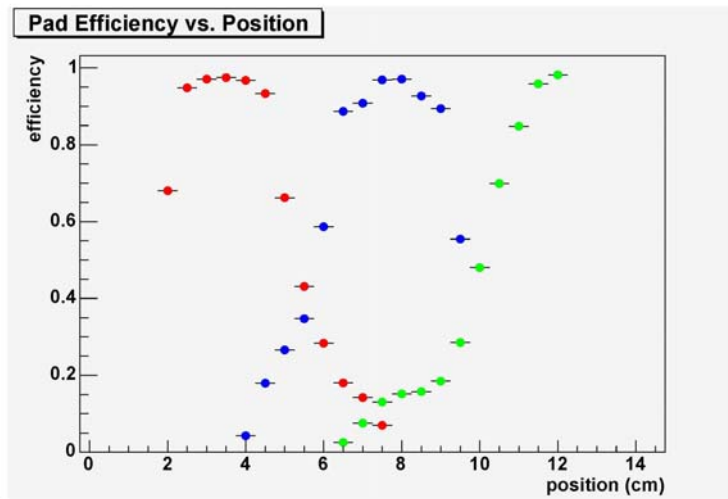

Figure 23. Horizontal scan across the pads of PH3.The efficiency as a function of hit position is shown.

The rest of the parameters studied, like gas flow rate, gas mixture etc did not have a significant impact on the MRPC performance. This means that the we can operate with a 2 component gas system and that it can have relatively relaxed tolerances on the exact Freon- isobutane mixture.

Three major goals were set for RUN5 :

- To investigate ways to improve the efficiency in the strip read-out design, while still running with a 2 component gas mixture. Wider strips were considered as a way to better contain the charge distribution and thus improve the efficiency. A new prototype with double –ended strip readout (PH4 shown in Figure 24) and 2 cm wide strips was built and operated during Run 5
- To build and test a complete electronics chain that operates with the PHENIX data acquisition system (DAQ).
- To evaluate of the performance of the different MRPC designs under heavy ion beam conditions.

5.a Run 5 set-up

Two identical gas boxes were installed in sector 0 in the West arm of PHENIX. The boxes contained the new PH4 chambers along with the already tested PH2 and PH3, which were included in the test to facilitate a fair comparison of performance under the conditions of heavy ion beams. Figure 25 shows a schematic view of the set-up showing the position of the read-out strips/pads (bottom of Figure 25). The top two photographs (Figure 25, top) show the detectors already installed on carriage. The prototypes were successfully operated for the entire duration of the Cu+Cu run. The low voltage, high voltage and DAQ chain were also successfully commissioned.

5.b Run 5 electronics R&D.

For the KEK test, we used pre-amplifier/discriminator boards designed for the STAR MRPCs at RICE University and used by STAR during RUN3. In the STAR documents, these are referred to as the FEE boards. Mechanically, these electronics consist of two layers of circuit boards. The "lower" level is the Feed-through boards (F/T). These gas-seal and faraday-cage the MRPC gas volume,and pass the MRPC signals out of the gas box and to the "upper layer", which are the "FEE" boards. The F/T boards do nothing more but complete the faraday cage about the MRPCs and pass the signals using IDC-style pin headers. These boards are very sparse in terms of components and do not require low voltage. Bleeder resistors are used on these boards to prevent pads from charging up if the FEE boards are not connected.

The FEE boards used in the KEK test have two outputs per MRPC readout

channel. One is a amplified copy of the original input signal (for digitization in an ADC), and the other is a NIM-standard logic signal (for a TDC).

The FEE board contains both pre-amplificiation and amplificiation of the MRPC signals. The preamp device, a Maxim 3760, is a low-noise-input trans-impedance integrated circuit whose gain and rise-time characteristics are well-defined by internal feedback. This part is commercially available for use as a photodiode receiver preamp in data communication applications. Several designs employing this chip have shown excellent timing performance when connected to actual MRPC pads - the Maxim 3760 has been used extensively for the past three years by both the STAR and ALICE TOF groups. An AD8001 is used as the amplifier. An ultra-high speed integrated circuit comparator, the AD96685, serves as a simple leading-edge discriminator with externally controlled threshold. This circuit has also been demonstrated successfully in the several generations of STAR TOFr systems.

During the KEK test, we use CAMAC ADCs and TDCs to record the signals from the MRPCs. We were able to obtain excellent timing resolution using the on-board discriminator and a CAMAC TDC. However, the CAMAC readout, although shown to work, is not compatible with the PHENIX DAQ, which is designed for a large scale experiment. It is desirable to use one of the already developed Front End Modules (FEMs) to interface the pre-amplifier boards to the data collection modules (DCMs) and to communicate with the timing and trigger systems. We would like to use the TOF FEMs developed for the scintillator-TOF installed in the East arm of PHENIX. But we can not just replace the CAMAC modules with the TOF FEM. The difference is that the TOF FEMs accept analog signal only and then discriminate it within the FEM. This requires that the analog signal out of the pre-amp has a well defined timing edge, but the amplifiers in the RICE boards were not optimized to allow a good timing measurement using the analog signal.

For our R&D studies in RUN5, the RICE group produced 5 different modifications to their original (RUN3) boards. These were tested on the bench at Nevis laboratory and with cosmic rays. The modifications included:

(1) Channel 1:
modified feedback and compensation to
increase the bandwidth of the amplifier "a lot".
the leading edge is now faster (steeper) than before.
        Pulse hight increase: factor 2.
        Saturate ~350 mV.

(2) Channel 2:
same as channel 1, except comparator
is disabled, which doubles the pulse height on

the analog output.
Pulse hight increase: factor 3-4.

(3) Channel 3:
modified feedback and compensation to
increase the bandwidth of the amplifier, but
not as much as for channel 1.
Pulse hight increase: factor 2.

(4) Channel 4:
same as channel 3, except comparator
is disabled, which doubles the pulse height on
the analog putput.
Pulse hight increase: factor 4

(5) Channel 5:
same as channel 1, but source back
termination resistor removed. analog output still
drives a 50 Ohm cable & load, but analog
pulse height is double the height compared to
channel 1.
Pulse hight increase: factor 4

(6) Channel 6:
no change.

Configuration (5) was chosen for RUN5 electronics. Scope traces comparing
the analog and digital results from (5) compared to the original (6) are shown
in Figure 26. Further documentation of the pre-amp test can be found at:

https://www.phenix.bnl.gov/WWW/p/draft/chujo/MRPC/publish/preamp_test_0
4.0819/

   The RICE group produced a total of 40 boards to be used in RUN5. The
FEMs for RUN5 were spares from TOF.E , plus – we borrowed 4 FEM boards
that were connected to slats at the edge of the fiducial area. The goal was to
obtain a reliable test the electronics that is decoupled from the detector tests.
We instrumented 128 analog output channels and 64 digital outputs. The
analog vs digital readout was successfully tested (see the results section).

(5.98 [152.0])

(.34 [8.5])

5X .12 [3.0]
BETWEEN COPPER

(4X ⌀.1875 [⌀4.8] THRU
PIN HOLE
FOR LOCATING
SIMILAR BOARDS)

.5]

(19.13 [486.0])

6X 21.69 [551.0]

6X 21.06 [535.0]
(ACTIVE AREA)

.32 [8.0]

(1.75 [44.5])

6X .79 [20.0]

SEE DETAIL—A

J

SHADED AREA IS
COPPER CLADDING
6 STRIPS

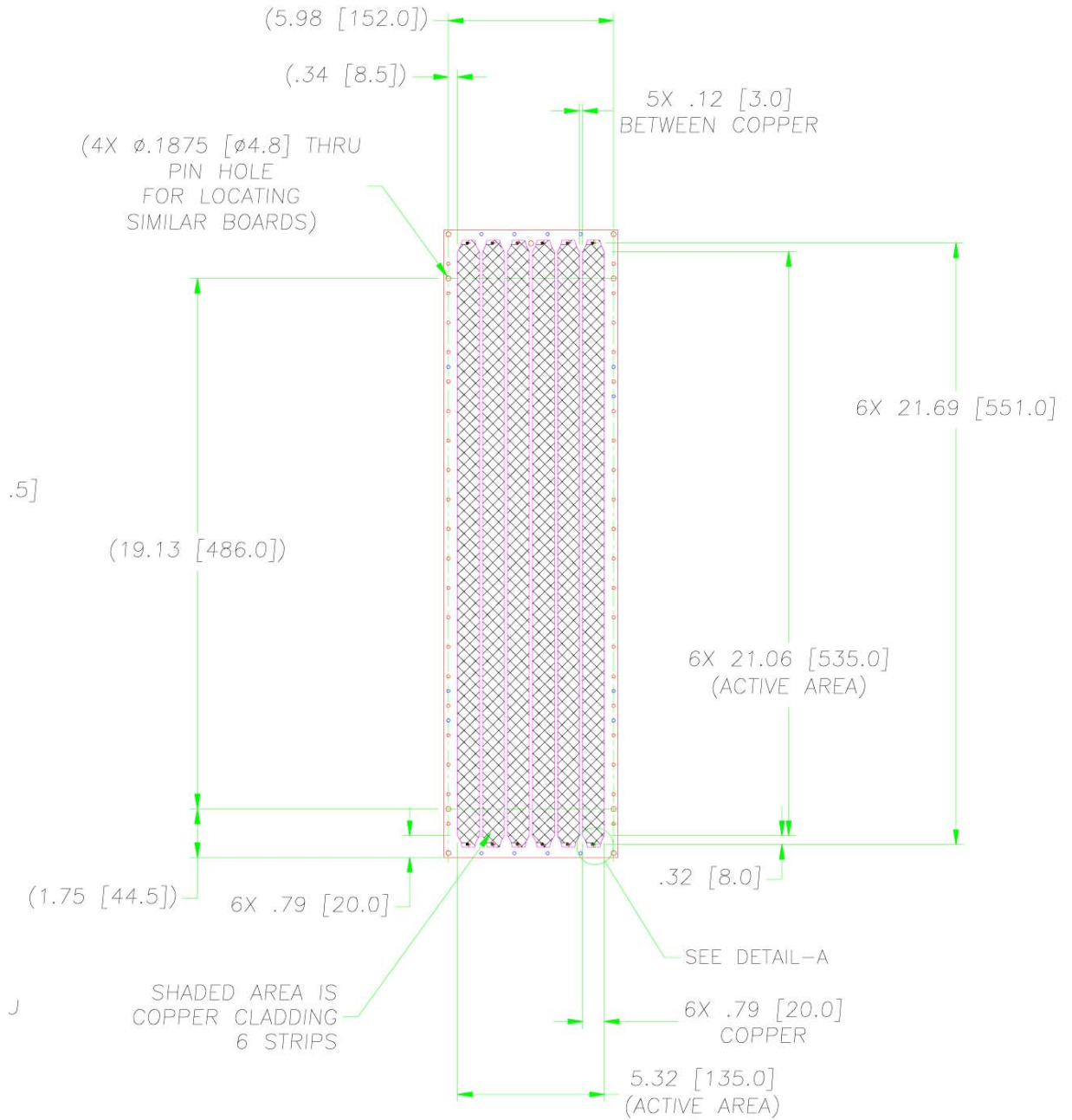6X .79 [20.0]
COPPER

5.32 [135.0]
(ACTIVE AREA)

Figure 24. PH4 pick-up strips design. The drawing in the figure was used to produce the PCBs for this prototype.
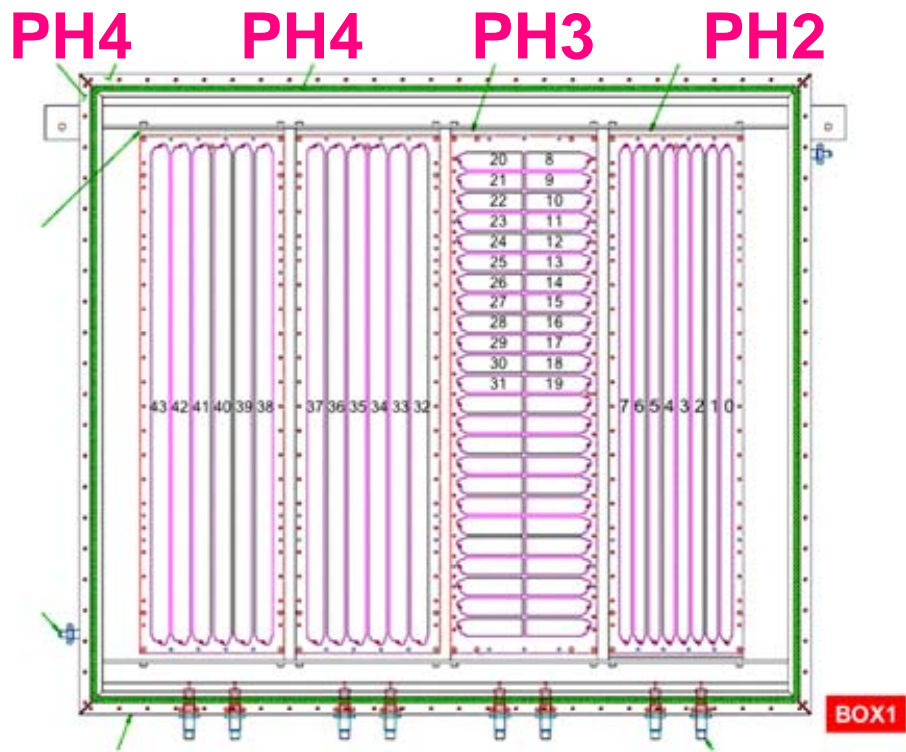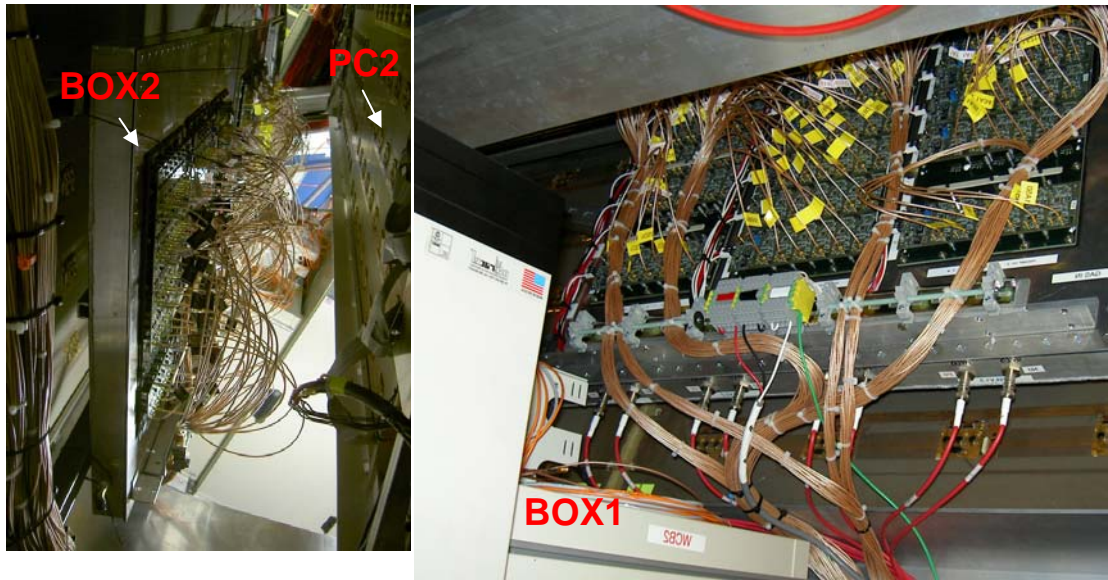
Figure 25. TOF West configuration in RUN5. Three different MRPC designs were operated in PHENIX during the Cu+Cu run. Two identical gas boxes were installed in sector W0 between PC2 and PC3 as shown in the photograph (top figure).
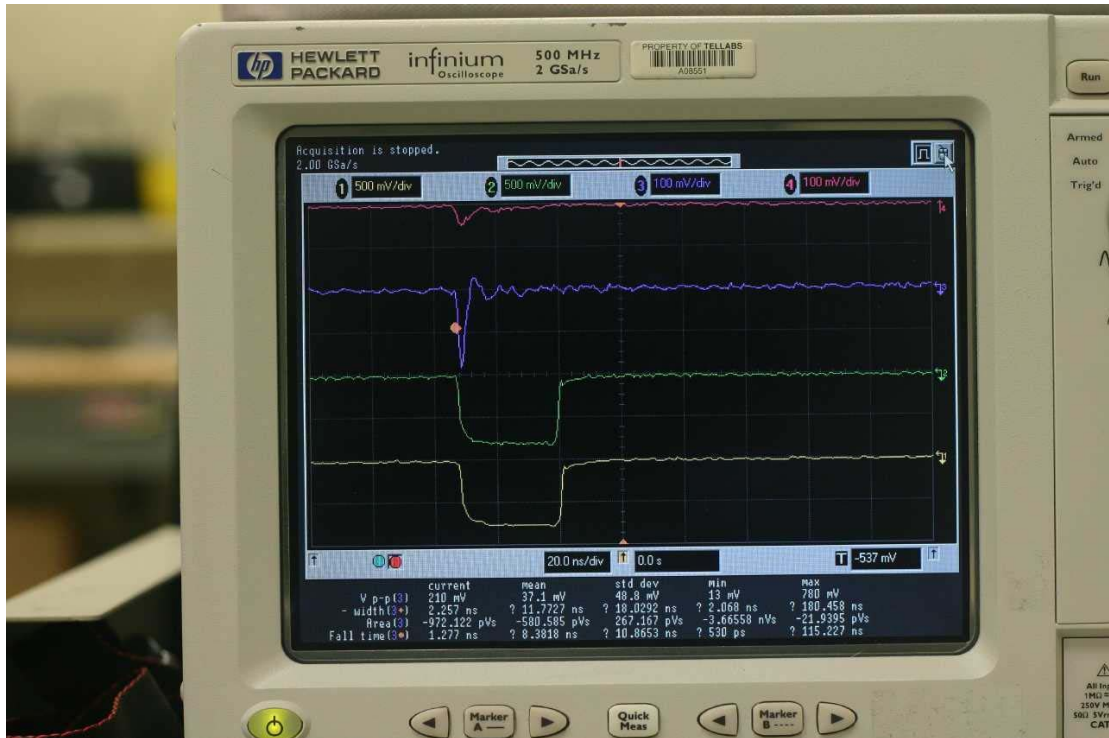
Figure 26. Pre-amp test with cosmic rays. Comparison between the RICE boards used in STAR during RUN3 and the boards used by PHENIX in RUN5. Scope traces:

- CH 1 (yellow): bottom picture, discriminated signal from UNMODIFIED preamp ch. 500 mV/div.
- CH 2 (green): 2nd picture from bottom, discriminated signal from MODIFIED preamp ch. 500 mV/div.
- CH 3 (blue): 2nd picture from top, analog signal from MODIFIED preamp ch. 100 mV/div
- CH 4 (red): top picture, analog signal from UNMODIFIED preamp ch. 100 mV/div.

5.c RUN 5 results

The TOF.W prototypes were installed in November 2004 and operated for the entire duration of the Cu+Cu run (until March 31st, 2005). During this RUN, we also commissioned the low voltage system and the high-voltage system, which we expect to remain without modifications in the future runs. A description of these systems is provided in the Section 5 (Conceptual design).

The data collected during RUN5 is not yet fully analyzed. A mini-production was carried out in order to study the timing resolution, the efficiency and to compare digital and analog readouts. Most of the data was taken with 15 kV high-voltage setting, which was selected based on the results from the KEK beam test. A voltage scan was performed towards the end of the running period. Data was taken at 14 kV, 14.5 kV, 15 kV and 15.5 kV. All voltage scan data was taken within a 24 hour period.

5.c.1 Electronics and resolution studies

The goal of the electronics studies in Run5 was to compare the timing resolution obtained using the analog output of the pre-amp, which is then discriminated within the TOF FEM, versus the on-board discriminator. In both cases, the analog signal is recorded and is used to determine the slewing corrections. The concern is that the analog signal will deteriorate in the long cables between the pre-amp and the FEM. We used RG316/U cable, 50 ft long with LEMO plug on one end and MMCX plug on the other end. This is certainly not the best quality cable available and the length that is needed in the final configuration is significantly shorter, so this test should be considered as the worst case scenario for the final system. One of the early runs was used for this study. Here we present the results obtained using one of the PH4 chambers.

The timing resolution of the PH4 chambers was measured in a standard way by selecting high momentum particles and forming the difference between the measured flight time and the expected flight time under the assumption that the particle is a pion. Calibrations included slewing corrections and slat-by-slat timing offsets. Slewing corrections were done separately for the analog and the digital signals. The slewing effect is much more significant for the analog signals and requires a careful calibration. Figure 27 shows the Time-T$_{expected}$ versus charge (ADC value) for one slat at the 15 kV HV setting. We found that the slewing curves depend on the applied high voltage and may also be affected by the percentage of streamers.
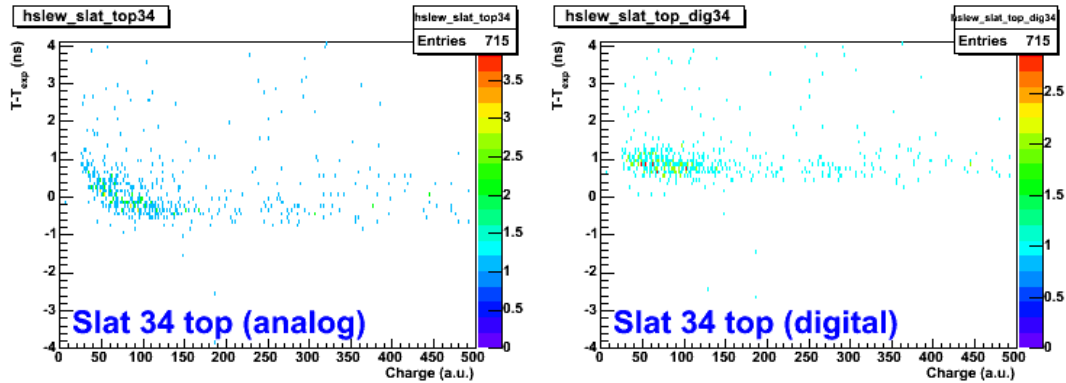
Figure 27. Time-Time_expected versus Charge (ADC value) measured with the analog (left) and the digital (right) read-out chain. The top read-out of slat 34 in PH4 chamber is shown. The voltage setting is 15 kV

Figure 28 and 29 show the momentum versus $T-T_{exp}$ distributions obtained for the analog and the digital signals before and after slewing corrections. Significant improvement in the width of the timing distribution is achieved after this calibration.
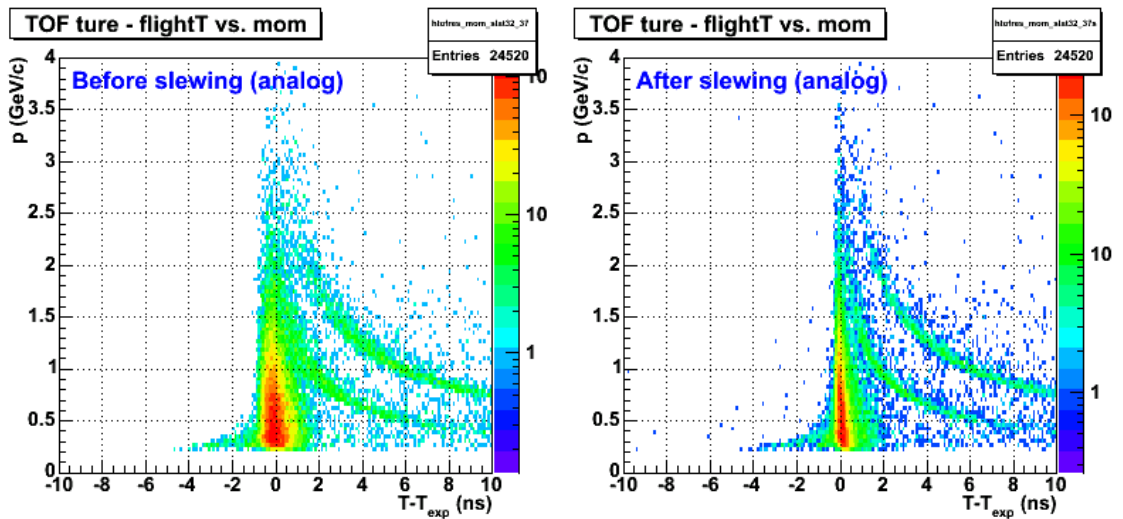
Figure 28. Momentum versus $T-T_{exp}$ distributions obtained for the analog signals before and after slewing corrections. Negatively charged particles are included.
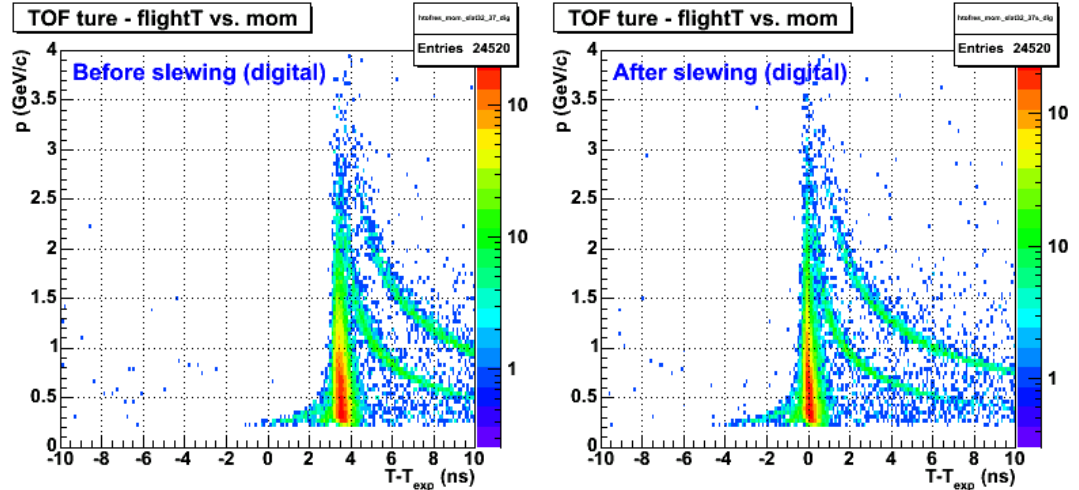
Figure 29. Momentum versus $T - T_{exp}$ distributions obtained for the digital signals before and after slewing corrections. Negatively charged particles are included.

These plots show negatively charged particles only, since the acceptance in the W0 sector is worse for the positively charged particles. The distribution of 1/velocity versus charge*momentum for both charges is shown in Figure 30. A clear π/K separation is seen for momenta exceeding 2 GeV/c. The p/K separation is difficult to judge from this plot, due to low statistics, but we expect that it will reach above p_T = 4 GeV/c.
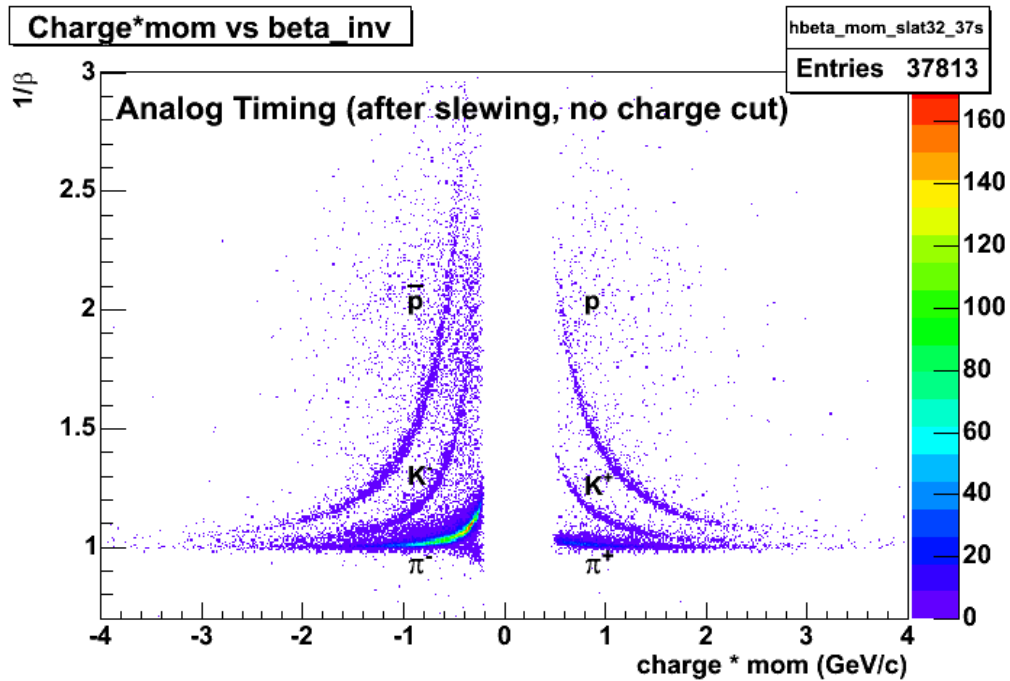
Figure 30. The distribution of 1/velocity versus charge*momentum obtained after slewing corrections (but no streamer cuts) with PH4 MRPC during the Cu+Cu run (Run 5 @ 200 GeV).

The plots in Figure 31 show the timing distributions for the two electronics read-out chains. We obtain comparable resolution from the analog and digital read-out, which gives us confidence that the electronics solution (modified RICE pre-amp + TOF- East FEM) is suitable for the full detector construction. The resolution in Figure 31 of $\sigma \sim 120$ ps was achieved after applying slewing corrections, but has not been optimized by cutting out streamer contribution. It also includes contribution from the start-time counters ($\sigma \sim 40$ps). Figure 32 shows the effect of a charge cut that eliminates the tracks that result in streamers. The resolution is improved by ~20 ps. After subtracting the contribution from the start-time counters, we obtain intrinsic timing resolution of $\sigma \sim 96$ ps, which satisfies our design goals.
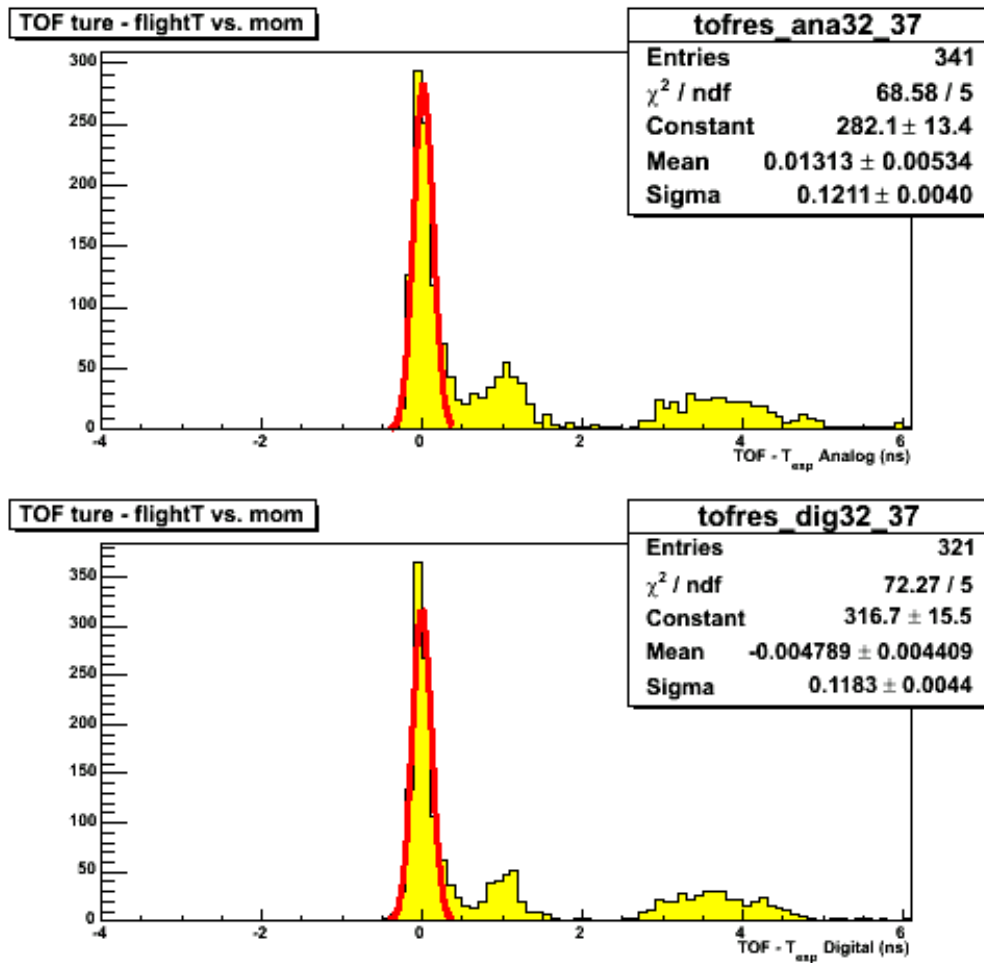
Figure 31:
- Timing resolution: with NO streamer cuts applied and no start time subtracted
  - **Analog: 121 ps (top plot)**
  - **Digital: 118 ps (bottom plot)**
- Comparable timing resolution between analog and digital signal.

ana_slat32_37sc

Entries	314
χ^2 / ndf	7.045 / 3
Constant	375.4 ± 15.1
Mean	-0.03242 ± 0.00382
Sigma	0.1096 ± 0.0031

Analog

π^-

1.2 < p < 1.5 GeV/c
w/ charge cut

σ_{TOF} = 109 ps

No start timing resolution subtracted

K^-

$\bar{p}$

TOF - T_{exp} Analog (ns)

dig_slat32_37sc

Entries	283
χ^2 / ndf	12.65 / 3
Constant	443.2 ± 17.1
Mean	-0.009712 ± 0.003457
Sigma	0.1008 ± 0.0027

Digital

1.2 < p < 1.5 GeV/c
w/ charge cut

σ_{TOF} = 100 ps

No start timing resolution subtracted

TOF - T_{exp} Digital (ns)

Figure 32. Timing resolution in the PH4 chambers after streamer cuts were applied. Analog and digital signals are compared. The contribution of the start time counter (σ ~ 40 ps) has not been subtracted.

The resolution was also studied as a function of position within the MRPC. The slat-by-slat results for one of the PH4 chambers are shown in Figure 33. The timing resolution for analog and digital signals is shown. The solid points Show the results without streamer cuts. The open points show the results after the streamer cuts are applied. In both cases, the start time resolution is not subtracted.
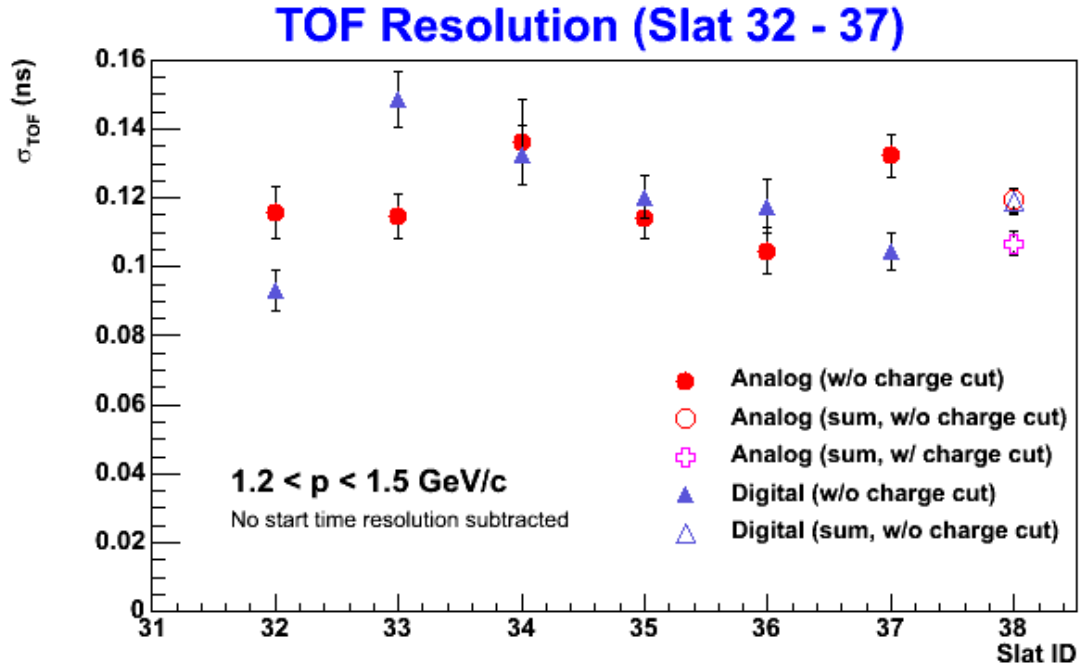
Figure 33 Slat-by-slat timing resolution in the PH4 chambers at 15 kV.
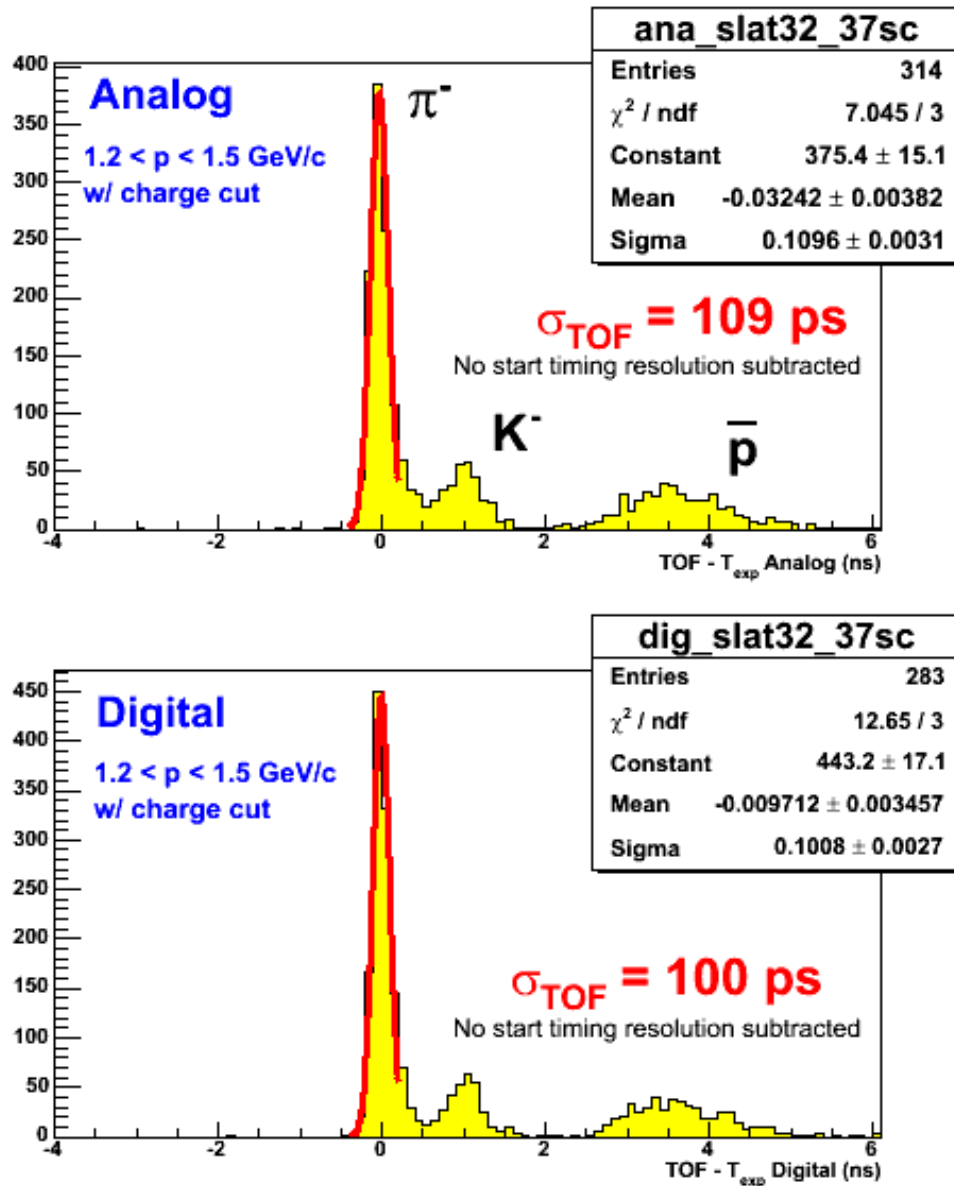

5.c.2 Efficiency studies

One of the goals for RUN 5 was to compare the efficiency of the narrow strip design (PH2) with a wider strip design (PH4) MRPC. Since the efficiency depends on the applied high voltage, we conducted this study using the high-voltage scan data. The efficiency of the MRPC was determined under the following conditions:

- Good quality tracks are selected from the drift chamber
- Tracks are matched with hits in PC2 and PC3 that are located in front and back of the MRPC, respectively. Cuts in PC3 -z are used to define the MRPC chamber which is expected to register the hit.
- The efficiency is determined as the number of hits in the MRPC associated with the tracks that pass the above selection divided by the total number of selected tracks.

The results for the efficiency obtained using two PH2 chambers and two PH4 chambers as a function of the applied high voltage are shown in Figure 34.
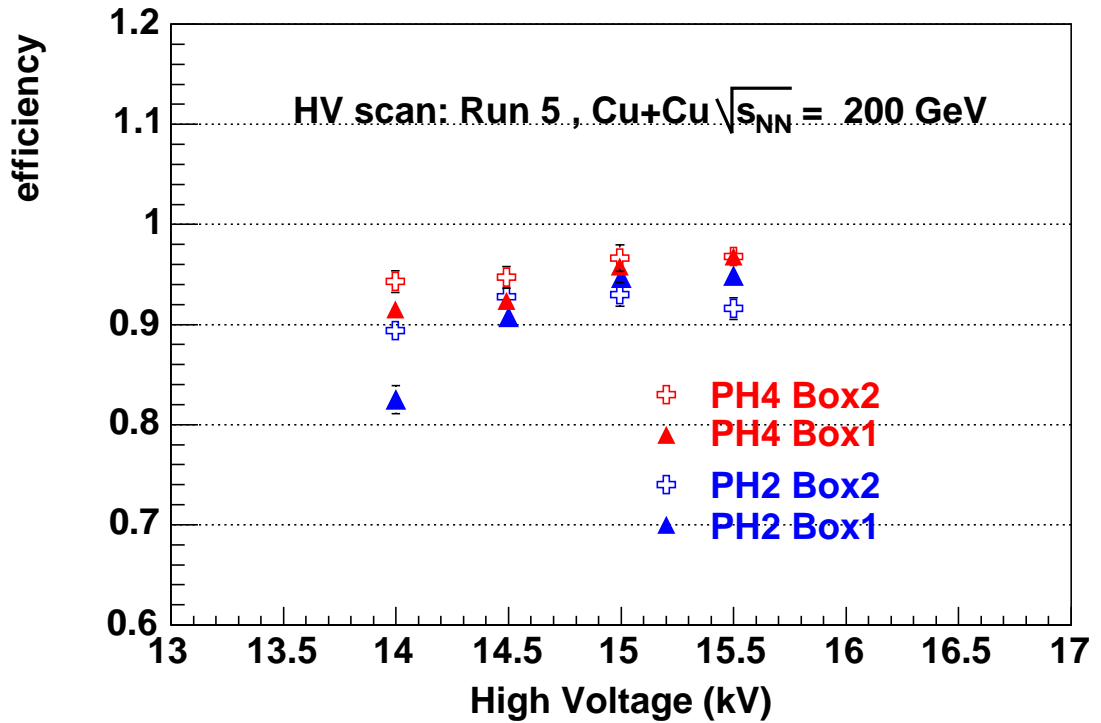
Figure 34. Efficiency study comparing PH2 and PH4 chambers in gas box 1 and gas box 2.

The blue point in the figure show the efficiency in the PH2 design, while the red points show the results for the PH4 chambers. The two sets of points (open crosses and filled triangles) correspond to the two different gas boxes. The PH4 chambers show efficiency in the range 92- 97% for voltage settings between 14 kV and 15.5 kV. The results obtained from the two gas boxes are consistent. The PH4 efficiency is systematically higher than the PH2 efficiency, although the difference is close to the level of the systematic error of these studies. In any case, we have confirmed that the wider strips perform at least as good as the PH2 design that was tested in KEK and possibly – about 2% better. We note that the 98 – 99% efficiency numbers quoted by STAR and ALICE were only achieved when using a 3 component gas mixture.

5.c.3 Operating conditions studies with heavy ion beams

For the most part of RUN5 the MRPCs were operated at 15 kV, which was determined to be optimal voltage setting in the KEK test. Voltage scan data at four settings was also taken towards the end of the Cu+Cu run. We studied the timing resolution, the efficiency and the streamer component as a function of high voltage. The data analysis is still ongoing. Here we present the first results from this study.

First we note that the slewing corrections apparently are voltage dependent, which is probably due to the gain change with HV. The second observation is that the timing resolution results obtained in the voltage scan data are worse by ~ 10 -15 ps compared to the results during the Run. This could be due to the fact that the MRPCs need longer conditioning after a voltage change, which was not done during this voltage scan. We also find a larger percentage of streamers during the voltage scan (for the same voltage setting of 15 kV). Figure 35 summarizes the timing resolution results from the voltage scan. The resolution was measured with and without the streamer contribution. We find that the resolution in the avalanche mode does not change within these voltage settings. The nominal operating voltage can be lowered from 15 kV to 14 kV. This will result in a better performance with a much smaller percentage of streamers.
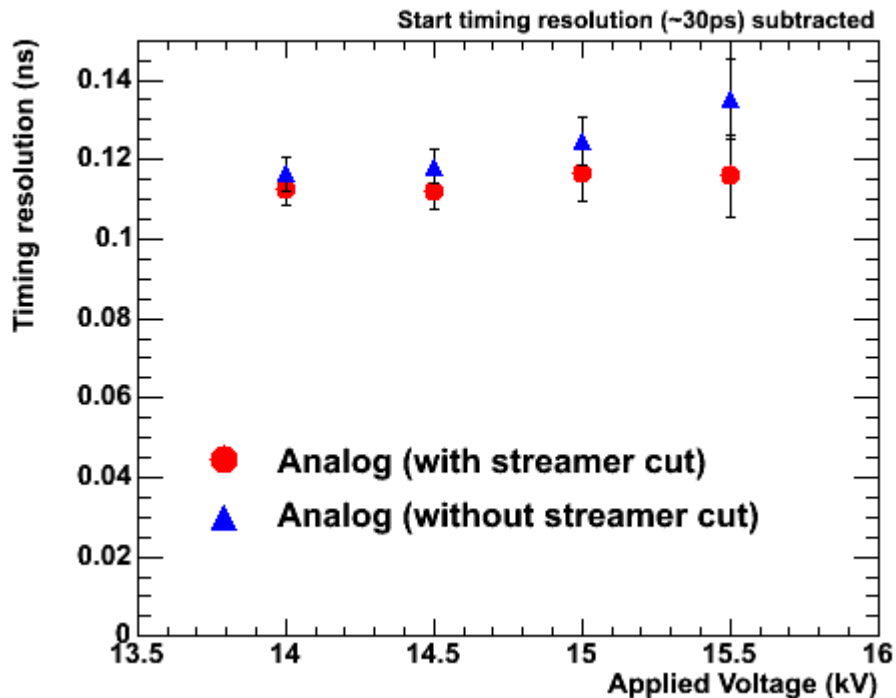

Figure 35. Timing resolution for PH4 as a function of applied HV.

The streamer contribution was measured during the HV scan and for the earlier Runs. Figure 36 summarizes the results. Unlike in the KEK beam test, the performance at HV > 14.5 kV with heavy ion beam has unacceptably high percentage of streamers. While the good timing resolution can be retained by cutting out the streamers, operation under these conditions is not desirable. One solution would be to lower the operating voltage. Another approach (used at CERN and elsewhere) is to add a small percent of SF_6 to the gas mixture. HV conditioning is also needed. We note that the 15 kV data in the voltage scan was taken just after the 15.5 kV data and the streamer contribution was increased significantly compared to earlier runs at the same voltage setting.
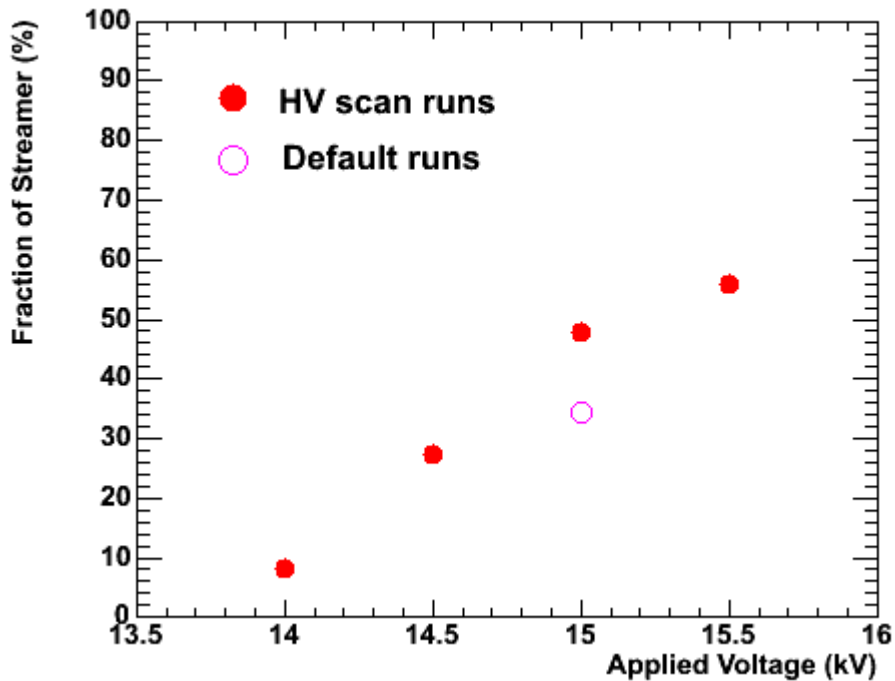
Figure 36, Streamer percentage measured in the HV scan during the Cu+Cu run.

To investigate the dependence on the environment and to test if the MRPC can recover after operation with very high streamer rate (such as at 15.5 kV), we evaluated the streamer component of the same chamber using cosmic rays at Vanderbilt after the detector was decommissioned. The ADC distribution at 15 kV is shown in Figure 37. The streamer component is reduced by a large factor in comparison both to the default runs and the voltage scan runs. We conclude that in the high multiplicity/high rate environment, the streamer contribution is increased and needs to be closely monitored.
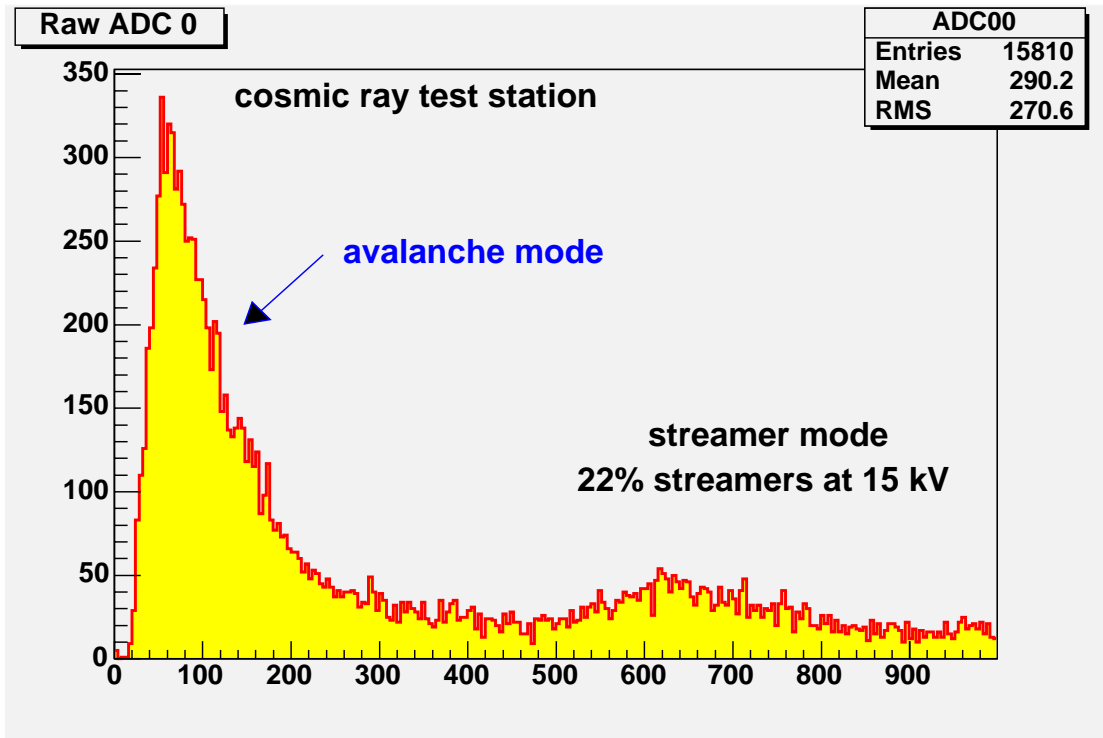
Figure 37. Streamer contribution measured with cosmic rays at 15 kV. The measurement was done after decommissioning the detector. No apparent damage was found.

as a continuation of our R&D studies. After the KEK test, the designs that remain under consideration are PH2 and PH3. We would also like to build strip chambers with wider strips (PH4) in order to improve the efficiency in the strip design. This evaluation is crucial for the successful construction of the full system for Run6. To achieve this goal we are planning to install 2 gas boxes, each approximately 55x55 cm^2 in sector W0. Box 1 will contain the new design PH4 chambers. In box 2 we will install 2 chambers of each PH2 and PH3. We will also test the performance of the full electronics chain. We hope to obtain valuable information starting from the beginning of Run5, such that the decisions can be made and the detectors can be built for Run6.

6. Conceptual design of the full TOF West system

The following conceptual design is based on our R&D studies tested at KEK and in Cu+Cu beams at RHIC (RUN5)

6.a MRPC design

The TOF West system will be constructed with single stack, 6 gap MRPCs. In order to optimize the coverage, the size of the chambers slightly different from the PH4 design, but the read-out strips will have the same active area (and occupancy) as the PH4 chamber. In the final design, the MRPCs will have 4 strips with double ended readout. The thickness of the glass and the gas gaps will remain the same as for the prototype detectors. Figure 38 shows a cross sectional view of the final chambers with all components and sizes included. Figure 39 shows the drawing of the PCBs. The drawing files can be found at:

http://www.phenix.bnl.gov/WWW/p/draft/julia/TOFWest/CDR/support
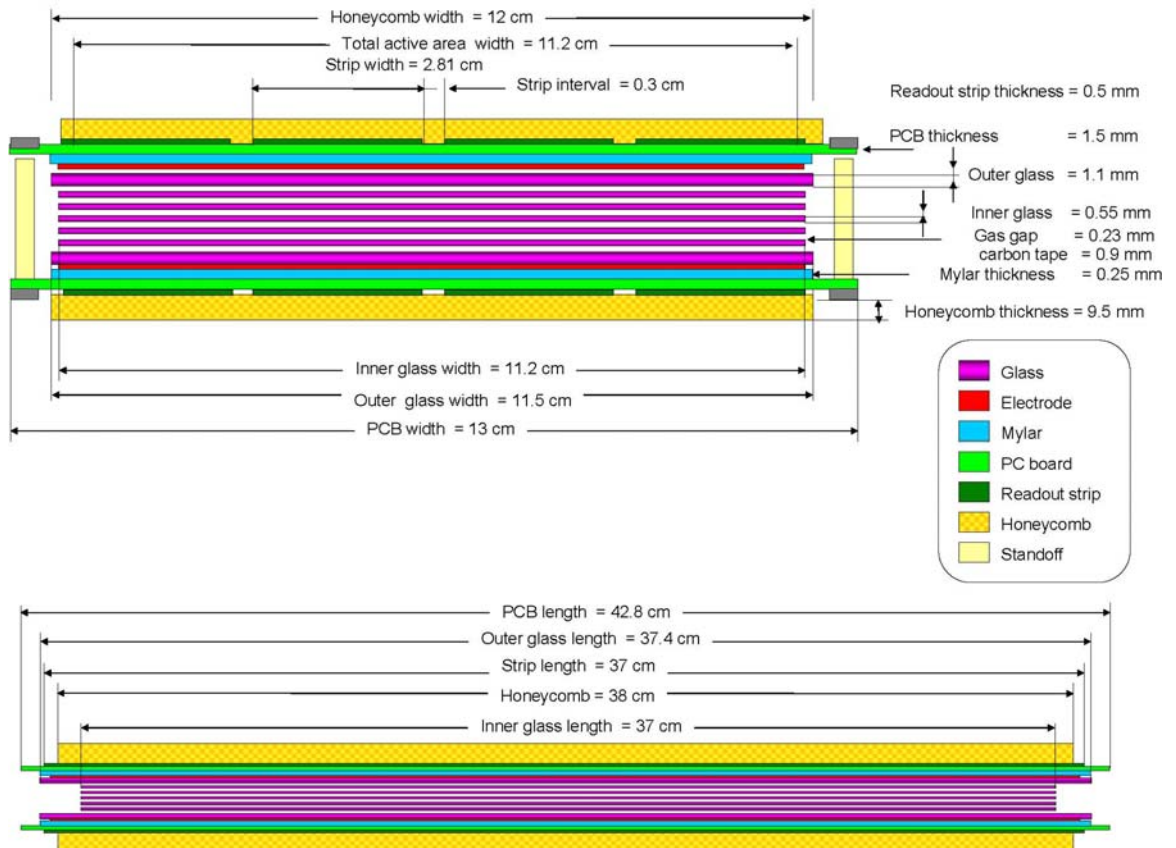

Figure 38 . Cross sectional view of the TOF.W MRPC to be installed in sector W1. All components and sizes are labeled in the figure. The two views are not to scale.
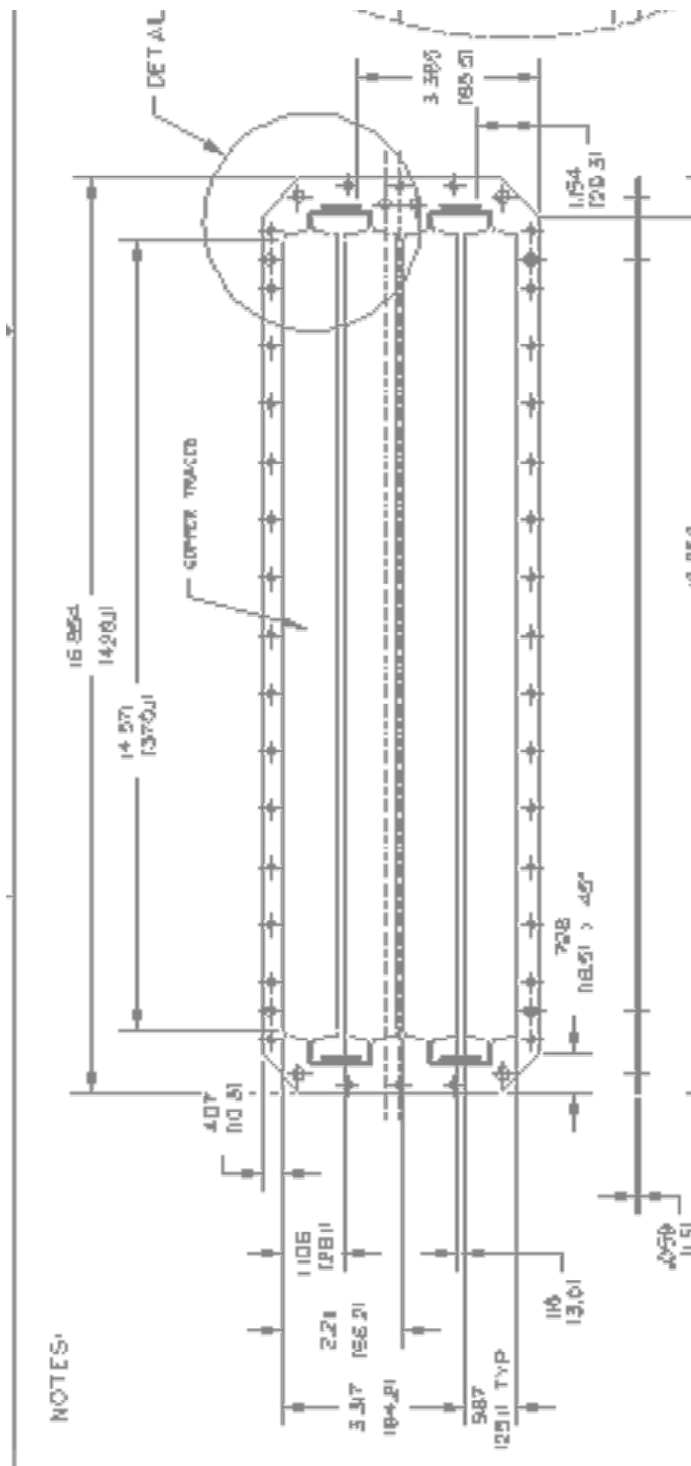
Figure 39. PCB drawing for the TOF.W MRPC showing the strip configuration and the connector footprints. A copy of this drawing is located at:
https://www.phenix.bnl.gov/WWW/p/draft/julia/TOFWest/CDR/support/PCB.pdf

6.b Mechanical design and integration

6.b.1 Description

The mechanical design of the Time Of Flight MRPC detector array to be installed in the West Carriage (TOF West) of the PHENIX experiment is driven by a combination of mechanical and structural constraints overlaying the prototype design which successfully demonstrated compliance with performance requirements. The new detecor will be comprised of 4 independent enclosures (panels), each of which house an array of detector modules and will be installed in a common plane, north and south, up and down. The area to be covered is roughly 4 meters wide by 2 meters tall, and as such each enclosure would be approximately 2 meters wide by 1 meter tall. The enclosures need to fit in a radial space outboard of the existing Aerogel detector, and it is desirable that the detector enclosures be installed without having to disturb any existing detectors.

The modules are essentially the same as the prototype PH4 module, which was determined to have the most desirable performance in the prototype detectors. The new modules have been modified in width and length so as to maximize the detector coverage within the inherent constraints of the 4 enclosures and the number of available signal channels (1024). Each module has 8 channels, 4 from each end and there are 32 modules per enclosure. The modules are arranged within each enclosure into 2 vertical halves with each half containing a checkerboard pattern of modules and spaces with an opposite pattern in the mating half so that detector coverage is maximized by overlapping the modules on one half with those on the other half.

Each of the detector modules has high voltage planes inside the enclosing pc boards which are distributed from 8 high voltage feedthroughs mounted on the vertical edges at the north and south ends of the detector space envelope. Signals from the modules are routed through pc board feedthrough connectors for each module hermetically sealed into one of an array of "pockets" formed in the radial outer and inner covers of each enclosure. Each module routes its signals to the adjacent pocket where a preamp is mounted. The preamps are to be inset into the pocket on standoffs which allow air to convect heat away naturally while positioning the preamps so that their components are within the pocket. Each preamp has 8 coax signal cables which are then routed to a patch-panel on the vertical edge of the north and south ends of the detector envelope space. Low voltage cables are daisy chained to the preamps from the patch-panel.

6.b.2 General Requirements

The general mechanical requirements which drive the design of the detectors and their enclosures are as follows:

a. Maximize detector coverage over the full vertical sector
b. Maintain gas tight enclosure using a mixture of 95% R134A/ 5% isobutane at 1.5 in WC internal pressure.
c. Size gas flow rate to achieve 5 volume exchanges per day
d. Gas is to flow uniformly through all of the detector modules
e. The module design is to be conceptually consistent with the prototype PH4 design, except that the plan view dimensions are to be scaled as necessary to achieve maximum coverage.
f. The detectors are to be packaged so as to fit in the annular space between the existing Aerogel and PC3 detectors on the West Carriage
g. There are 1024 signal connections, 32 high voltage connections, and 8 low voltage connections evenly distributed among the detector enclosures.
h. The detectors are to be designed to meet all applicable BNL safety requirements. Specific areas of concern include flammable gas and high voltage and material handling safety associated with the installation of the detectors.
i. Alignment   requirements:

Precision: X,   Y,   Z   :   +/-   1.0   mm
pitch,   roll,   yaw   :   +/-   1.0   mrad

Repeatability: X, Y, Z : +/- 1.0   mm
pitch, roll, yaw : +/- 1.0 mrad

Stability: X,   Y,   Z   :   +/-   .05   mm
pitch, roll, yaw : +/- .05 mrad

6.b.3 Tradeoff Studies

There were several mechanical design aspects for which multiple options were considered. Enclosure materials, preamp location (inside or outside the gas volume), module layout and dimensions, signal, low voltage and high voltage feedthroughs, distribution and internal routing, structural support and enclosure rigidity, and methods of sealing for gas were considered separately and collectively. The various options were considered for cost impact, relative reliability, and safety within the constraints of the general requirements. The tradeoff studies culminated in the design presented herein.

6.b.4 Construction Materials

The enclosure is comprised of two similar halves with formed aluminum 6061-T6 1.5 mm sheets for the end covers and aluminum 6061-T6 rectangular blocks 19 mm thick and 35 mm high. There are aluminum 6061-T6 rails which run longitudinally at the top, bottom and center of the enclosure halves to support the modules. These components are bonded with adhesive (Scotch Weld DP-460 or equivalent). The 2 halves will be sealed by a BUNA-N gasket.
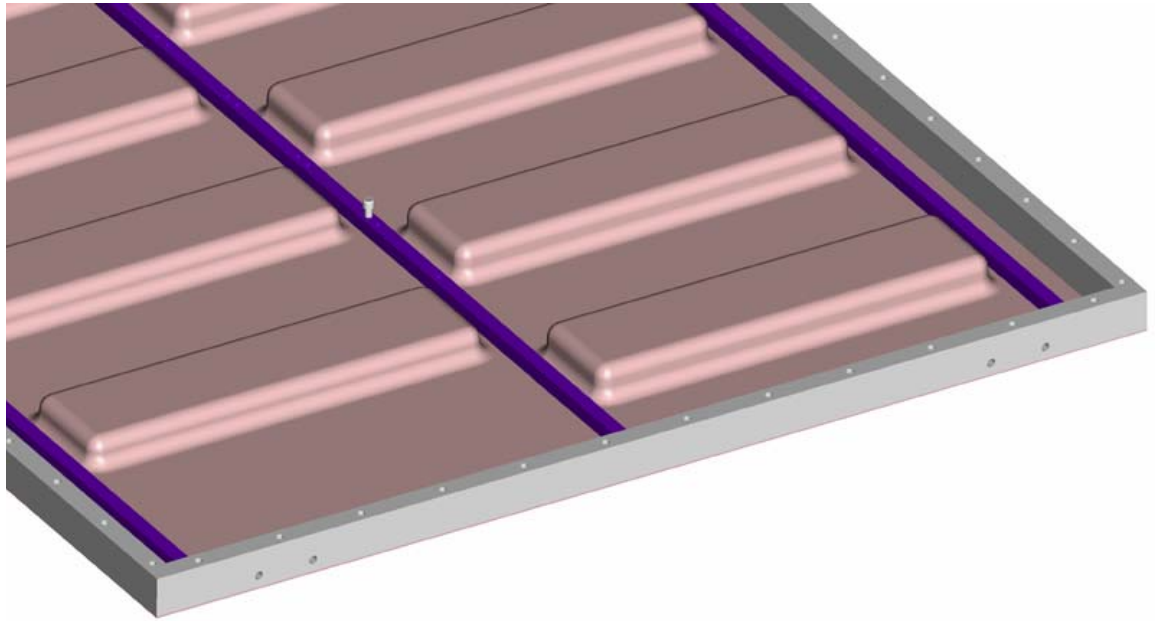
Figure 40: Half of Detector enclosure structure

6.b.5 Mechanical Layout of Detector Modules

The internal layout of the modules is in a checkerboard pattern of modules and spaces for each half of each of the enclosures. The mating half has its modules in a complementary pattern such that the modules fully a maximized area for each enclosure equal to the plan area minus space around the edges of the enclosure for structural, mounting, gas distribution and high voltage cable routing , signal wire connection and routing and a strip along the longitudinal centerline for signal wire connection and routing and module mounting. In total the, detector active area is **74** % of the total plan area of the enclosures, and **75** % of the available active area for the horizontal sector of the west carriage.
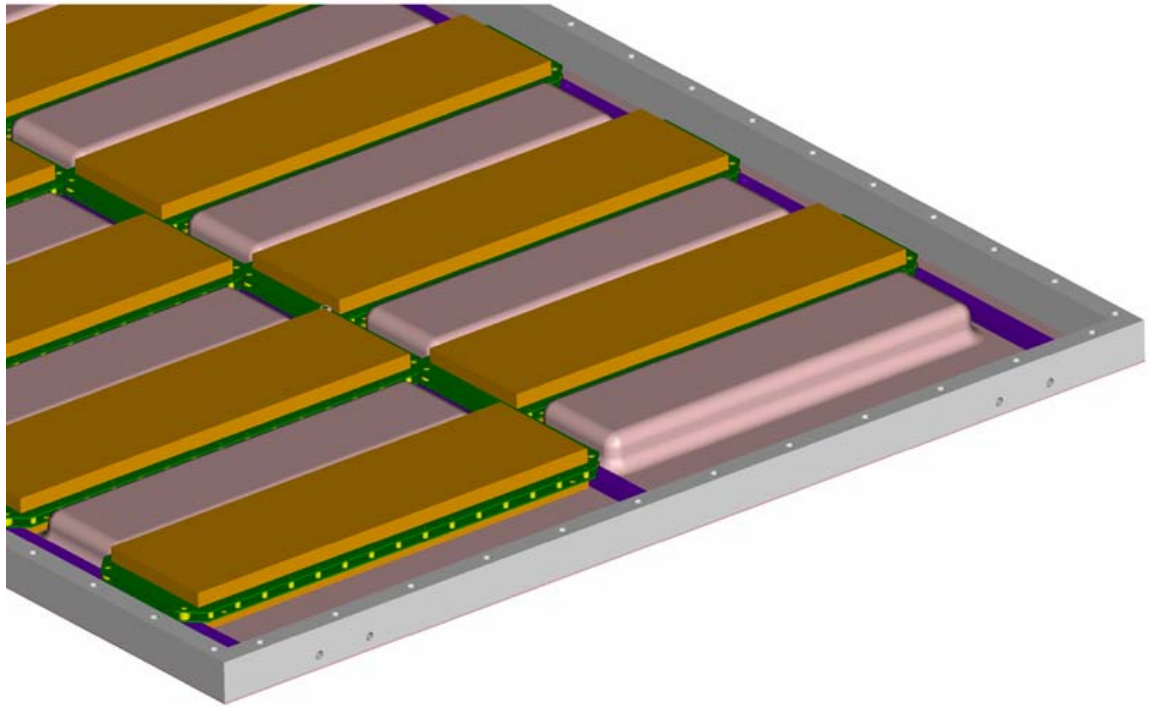
Figure 41: Detector arrangement within enclosure structure in half of an enclosure. Other half is mirror image.

Each module is comprised of a rectangular "sandwich" stack of components as follows:

Upper and lower pc board
Upper and lower 0.100 mm double sided tape
Upper and lower 0.250 mm mylar
Upper and lower 0.090 mm carbon tape
Upper and lower 1.10 mm thick outer glass
5 layers of interior glass each 0.55 mm thick, each glass layer is spaced 0.23 mm from adjacent layers by nylon "fishing line" which is routed serpentine from side to side around nylon standoffs.

Figure 42: Side view of module stack

6.b.6 Internal Gas Distribution

Gas will be distributed within the enclosures by means of 4 perforated tubes extending the horizontal length of the enclosure, with the perforations sized appropriately for uniform flow through all detector sections. One gas supply side will be at the bottom of each enclosure half and one return will be at the top of each half.

Figure 43: Detector enclosure with gas distribution piping and guide rollers. (Note: holes in distribution manifold are rotated 90° from normal orientation for illustration purposes)

6.b.7 Installation

The detector will be installed "garage door style", 2 enclosures (arranged north and south) at a time. The inboard/outboard and up/down symmetry designed into the detector enclosures will allow the enclosures to be arrayed so that the 2 panels to the north of the detector space will have their connectors and patch-panels facing north, while the southern end panels will be opposite. Tracks to guide the panels into their assigned space between the Aerogel and PC3 detectors will be made of 4 inch x 1.1 inch "C"-channel aluminum mounted on the interior side of the West Carriage towers. The 2 enclosures will be bolted together at the mid plane and stiffened laterally by a 3 inch aluminum I-beam and a ¼ inch aluminum connector plate. (The I-beam is on the bottom and the connector plate for the 1st 2 panels and the opposite for the remaining 2 panels.)
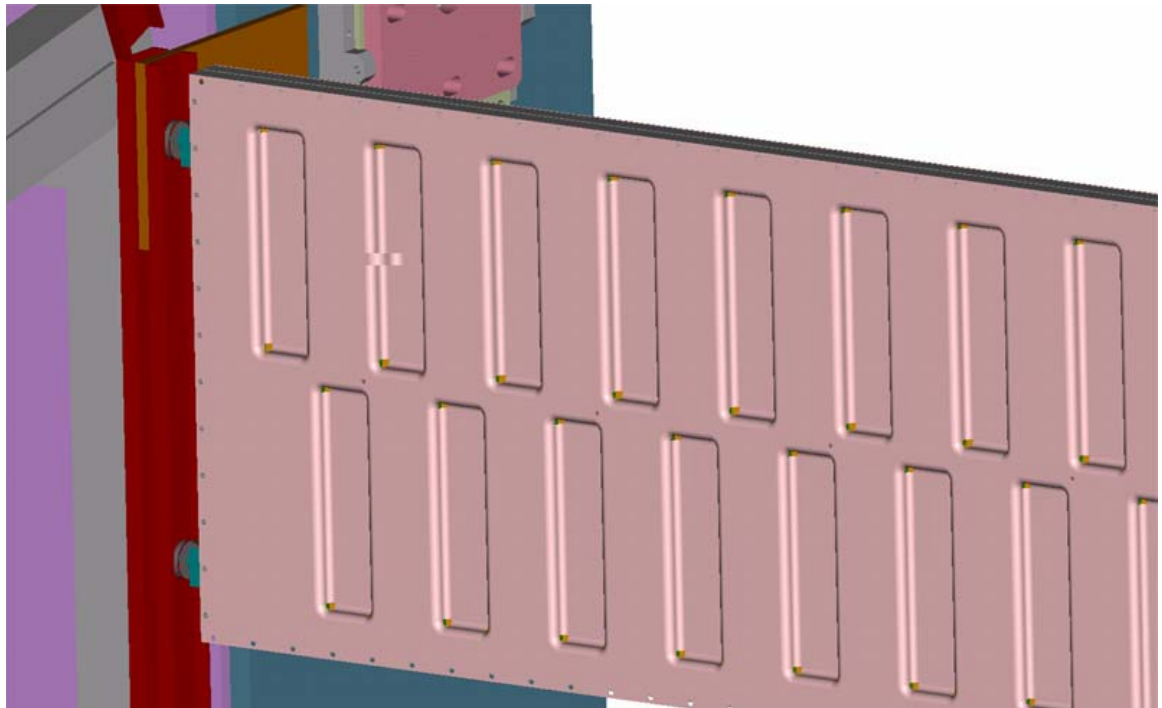

Figure 44: Illustration of enclosure panel with guide rollers in guide track. (Note: preamps in panel cover wells and wiring omitted for illustration purposes.)

6.b.8 Alignment and Survey

On each of the panels there will be 6 external fiducials (3 on each enclosure half) to which each internal module will be related before the enclosure halves are mated. Internal alignment to the required precision is accomplished by close tolerance machining of mounting components and precise positioning of machined components with fixtures prior to application of adhesive.

Each of the panels will have external fine adjustment provision in each of three mutually perpendicular directions. After the panels are lowered into place on the guide rails, the panels will be surveyed from their external fiducials and fine adjustments in each orthogonal direction will be made to align the panels to with specification. The panels will then be locked in their final positions.

6.c Electronics

6.c.1 Pre-amp electronics

The MRPC detector signals are imaged on copper pick-up strips and readout on both ends. The signals will be pre-amplified using modified version of the RICE feed-through and pre-amp boards. The schematics of the pre-amp boards before the modifications is available at:
http://www.phenix.bnl.gov/WWW/p/draft/julia/TOFWest/CDR/support/Amp Disc6.pdf
The final boards will include the analog part only. The revisions to the analog part of these boards are discussed in the previous section. These include the removal of a back termination resistor, as well as modifications to the feedback to the amplifier to improve the rise-time of the analog signal. This version of the RICE boards was successfully used in RUN5. In the final design, the digital part of the boards will be removed. The boards will be laid out with 8 channels to match the segmentation in the MRPCs. The connectors will change as follows:

- change single large ribbon cable header on MRPCs into two 8pair ribbon headers. Allows either single or double pairs per pad, plus empty ground pairs in between to reduce any possible cross-talk.
- thecable path off FEE is: Right-angle MMCX through-hole mounted jacks -> mmcx plugs on RG-316 to TOF.W patch panel-> Fujikura RG-58C/U -> FEM

Note that the new cable path is shorter and we use better cables than in RUN5. A comparison between the RUN5 and RUN 6 cables is shown below:

-- RUN6: Fujikura RG-58C/U (attenuation dB/km)
1MHz   14
10MHz   48
30MHz   81
100MHz   160
200MHz   230
2000MHz   900

---RUN5: Belden-e 84316 M17/113 RG316, MIL-C-17 55494
http://www.beldencable.co.kr/belden/more/84316.htm
(attenuation dB/km)
1MHz   39.3
10MHz   88.5
100MHz   272
200MHz   393
1000MHz 951

There is about factor 2 bigger attenuation in Belden cable.

6.c.2 Front-end-Module

The TOF West FEM has the same structure as the TOF east FEM. Each channel in the FEM performs both timing and charge measurement every beam clock cycle. The timing measurement is done through a time to voltage converter (TVC). The TVC use the discriminated PMT pulse as start and beam clock as stop. There are 2 clock cycle dead time after the discriminator fired. A continuous charge integrator (QVC) is used to measure the charge. The measurement will be stored in the switch capacitor array (SCA) every beam clock cycle. The SCA is used for both level 1 delay and multi-event buffering. Two custom chips are designed for the QVC+SCA and TVC+SCA circuits. When receive the Level 1 trigger accept, the trigger event charge and time data will be readout. 12 bits ADC is used to digitize both charge and time measurement. There are 16 channels per FEM card. Each TOF crate will host 16 FEM card. A crate interface is used to send data to the Data Collection Module (DCM) and to receive slowdown data from ARCNET. The ARCNET is used download soft parameters in the FEM, included the discriminators level, charge inject level etc. A timing interface module is designed to interface with the GTM. It receive the timing signals , L1 trigger etc, from the fiber from the GTM as well as recover the beam clock from the GTM fiber. Test pulse is generated by using 64 times the beam clock signals.

The clock and test pulse is send to timing fan-out modules. The module fans out these signals to 16 FEM and interface module.

The TOF FEM is designed in the early '90. There are two problems to fabricate the TOF west FEM,

1) 10 wafers were built for the two custom chips. 5 were used for the TOF FEM. We need to package additional wafer for the TOF west FEM. We will also need to rebuild the test fixture for the custom chips.
2) The SCA address line drivers and two of the analog device OPAMP on the TOF FEM are no longer been produced. We need to find the replacement parts and revise the TOF FEM design. As usual we need to have one prototype run to verify the new design.

The schedule is mostly driven the steps we need to take to deal with these two problems. A revised TOF FEM layout/prototype/test will take 3-4 months after being funded. The same amount of time will be needed to get chip packaged. 6 Months will be needed to produce all the 64 FEM needed to for the TOF West system.

6.d Low voltage

The low voltage supplies and cabling will remain the essentially the same as in Run 5, except – the channel count will increase. The schematic view of the LV system is shown in Figure 45. Four panels of TOF.W will be powered by 2 power supplies (one on each side) using 8 LV distribution cables (2 per side). To reduce the height of the pre-amp boards, the MOLEX connector on the pre-amp side may possibly change to mount screw-posts, plus simple crimp lugs on cable, to run LV from board to board.

The LV control has already been implemented in the standard PHENIX LV control system during Run 5. Figure 46 show the LV control panel , which will remain the same in the full system.

Figure 45. Low voltage supply and cabling for TOF.W.

Figure 46. Low voltage control panel including TOF.W was operated already during Run 5.

6.e High voltage

The high voltage system uses 2 CAEN SY127 mainframes (one on each side North and South). One mainframe was operated successfully in Rum 5 (See photograph is Figure 47). This is 40 channel mainframe. We will use 16 channels (4 out of 10 slot) on each side. The modules are CEAN 631 P and CAEN 631N . The technical specifications are given in Table 1. To meet BNL safety requirements, the supplier builds these modules using KINGS 1064-1 connectors (10 kV rated) instead of the standard SHV connector.

In Run 5 we operated each MRPC with its own HV supply. This is prohibitively expensive for the full system. Since the MRPC perform stably even in streamer mode, it is safe to combine several MRPC on the same HV bus. This is routinely done in the STAR TOFr tray, where 28 MRPCs share the same HV channel. In ower case – the modules have a roughly a factor of 4 bigger area and the total leakage current is higher by that factor. We have chosen to connect 8 modules to the same HV channel, which matches ower segmentation and specifications. There will be 8 HV connections in each TOF.W panel – 4 positive and 4 negative. Total of 32 HV cables will be run to the HV mainframes (16 on each side North and South). During Run 5 we used Reynolds 167-2669 cable with KINGS 1065 connectors. It turned out that this cable does not have the appropriate fire rating and will be replaced with a cable that meets these requirements (currently under investigation).

Figure 47. CEAN SY127 mainframe and A631P and A631N modules in RUN 5. The same configuration will be installed on each side of the TOF.W detector.

Technical Specifications Table

Vout full scale	8 kV
Iout full scale	40 µA
Voltage resolution	2 V
Current resolution	10 nA
Ramp up/down	500 V/s
Max ripple pp	<80 mV

Table 1. CAEN A631 P and A631 N modules technical specifications.

6.f Gas system

The Phenix TOF Gas System supplies 95%R134a+5%i-Butane mixture to the Time of Flight West (TOF.W) chambers at a controlled pressure. This system can regulate the flow rate of mixture while monitoring mixture temperature, flammable gas content, Oxygen and Moisture. A computer control/data acquisition system collects and logs the gas system operating parameters while providing a means of remotely controlling system valves.

6.f.1 Introduction

The primary purpose of the TOF Gas System (Fig.48) is to provide 95%R134a +5%i-Butane mixture to the TOF chambers at the correct constant pressure. Refer to Table 2 for a list of gas system parameters.

Mixer

CV3
CV6 O2 FI3
CV5 H2O FI4
CV4 i-Butane FI4
Analyzers
CV7
FI5

MV6   1/4"   80"WC   FI15   To vent
SV5
SV6   BPCV1

TIC 1   SV8
TC   PURIFIER   MV2
HE1   TIC 2   MV3
DRYER   PBV1
F3   PT 4
SV7

PIT 1

CV8   CV9
MV1
C1   C2   To vent

PIDC   PT 3   PIS 1
0.4"WC

CV1   CV2
FI 1   FM 1   FM 2
SV1 (n/o)
SV2 (N/O)   SV3
PT 1   PT 2
PI 1   PI 2
F1   F2
15PSIG
R134a   Isobutane

PCV1   FI16
BPCV2   FI11
FI7   TOF 1   PIT 4   OVF1
PIT 2   Bubbler 1   FI12
FI 6   FI8   TOF 2   PIT 5   OVF2
TT 1   Bubbler 2   FI13
BP   FI9   TOF 3   PIT 6   OVF3
PIT 3   Bubbler 3
1/2"   PT 8   FI14
F4   FI10   TOF 4   PIT 7   OVF4
Bubbler 4

TT 1   PIT 8
SV9(n/o)   1"   To vent

PCV-pressure control valve
SV- solenoid valve
MV- manual valve
CV- check valve
FM-mass flowmeter
FI- flow indicator
PIS- pressure indicating switch
TT-temperature transmitter
F- filter
PT-pressure transmitter
PIT-pressure indicating
    transmitter
C-compressor
PI- pressure indicator
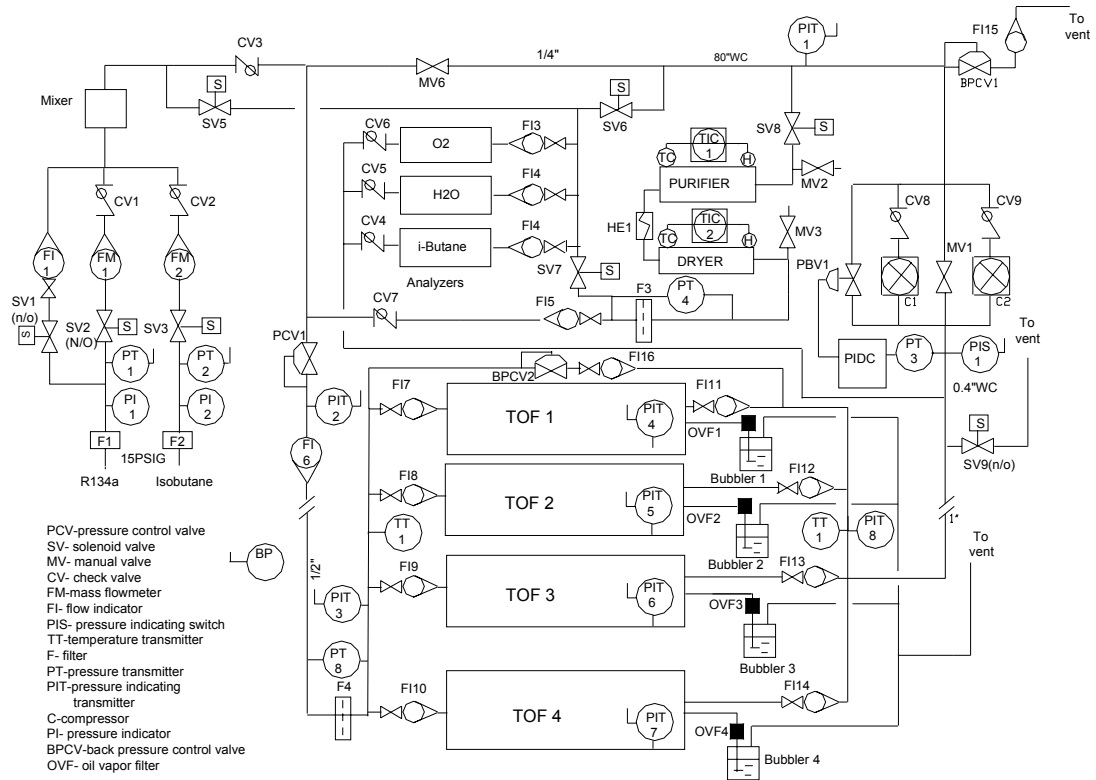BPCV-back pressure control valve
OVF- oil vapor filter

Fig.48 PHENIX TOF chambers Gas System

The system operates nominally as a closed circuit gas system with the majority of the gas mixture recirculating through the TOF chambers and delivery system. During normal operation, a small amount of fresh mixture is added and equivalent quantity of the return mixture is vented. The gas system can also be operated in a single pass open system configuration for purging.

The mixture circulation rate through the small membrane compressor is about 10 LPM at 80" H20 pressure. The gas system uses two compressors (C1, C2), one active and one set up as a backup. The gas from the compressors returns to the supply line through the check valves CV8 or CV9 depending on which compressor is active. The 60" H20 output pressure from the compressor is reduced to 30" H20 pressure by a pressure regulator (PCV1) before returning to the chambers. The compressors output pressure level is maintained with the back pressure regulator (BPCV1).

The return gas manifold is maintained at 1" H20 pressure above atmospheric pressure by a differential pressure transmitter (PT3) and electro-pneumatic PID Controller (PIDC) that operates bypass valve (PBV1). The bypass shunts flow from the compressor discharge line directly back to the compressor's inlet. A second manual bypass valve (MV1) is adjusted to enable the automatic control loop to be used within its optimum range.

The bypass line which includes the back pressure control valve (BPCV2) gives the possibility for a smooth gas system start. It also provides means for

a rapid response to increased or reduced i-Butane content measured with the i-Butane analyzer upstream of compressor.

Two flow indicators (FI6 and FI16) will measure the recirculating flows: main and bypass. The difference between them is the flow through the TOF chambers.

A measurement of the fresh mixture (FM1, FM2) into the system and flow vented through the flow indicator FI15 will give an estimate of the system leak rate.

The purity and composition of the mixture is monitored using oxygen, i-Butane and humidity analyzers. A fraction up to all of the recirculating mixture can be passed through a purifier and dryer to remove moisture and oxygen contaminants as needed.

A computer driven data acquisition/control system monitors all of the process variables. The computer system flags quantities which fall outside of predefined limits and initiates corrective action. The computer system also transmits an alarm to the Phenix crew to alert them of any problems.

It is imperative, for the safety of the devices, that the TOF chambers inside pressure accurately tracks barometric pressure. A rapid change in atmospheric pressure is typical preceding storms and hurricanes. To assure that the TOF chambers follow a fast rise in atmospheric pressure, a relatively large flow of inert gas will admitted into the TOF chambers in the event that normal pressure controls fail to keep up with "falling" internal pressure. The vent lines and associated valves are sized to allow for rapid venting of the TOF chambers mixture to prevent a high internal pressure in the case of sudden barometric pressure drops.

Table 2. Performance of Gas System is as follows:

Mixture	(95%R134a+5%i-Butane)
Compressor pressure	40-80 " H_2O
Supply pressure	30"+/-0.05 H20
Return pressure	1" +/-0.05 H_2O
Recirculation flow	650-1000 ccm
Mixture flow through TOF chambers	850 ccm
Purge flow	2.5 l/m
Make-up mixture flow	100-300 ccm
Oxygen content	< 500ppm
Water content	<100ppm

6.f.2 Pressure Control

There are two sources of pressure in the system: the first is the compressors located at the return from the TOF.W chambers. The second is the flow of fresh gas through the mixing manifold at the input of the system. Nominally the pressure within the TOF.W chambers is controlled by maintaining a constant pressure upstream of the TOF.W via the pressure reducing regulator (PCV1) plus back pressure regulator (BPCV2) and varying the pressure downstream of the TOF.W chambers by regulating the amount of mixture shunted from the compressor output to inlet (measures at PT3). On a longer time scale the flow of fresh mixture is constant.

The output from the compressor is 650 to 1000 ccm at 60" H20 pressure. A back pressure regulator (BPCV1) in the outlet line is set to 80" H20 pressure thus maintaining a maximum delivery pressure independent of the compressor's output. This pressure is reduced to 30" H20 pressure by the pressure regulator (PCV1) and supported with the back pressure regulator (BPCV2) upstream of the TOF.W chambers. The TOF.W chambers exhaust pressure, measured at the return gas manifold is maintained at 1" H2O pressure by a TESCOM ER3000 electro-pneumatic PID controller. A 0-2" H2O differential pressure transmitter (PT3) on the return manifold produces a 4-20 mA output that the PID controller compares to a set-point value. If the transmitter signal is different from the set-point, the controller sends a pneumatic output signal to the bypass control valve (PBV1). The bypass shunts flow from the compressor discharge line directly back to the compressor's inlet. Opening the bypass valve causes the TOF chambers exhaust pressure to rise and closing the valve makes the pressure fall. A second bypass valve (MV1), manually adjusted during the initial system set-up, enables this automatic control loop to be used within its optimum range.

The fresh mixture is admitted between the pressure regulator (PCV1) and back pressure regulator (BPCV1). The quantity of fresh mixture can be adjusted in the range of 100-3000 ccm with the mass flow controllers (FM1, FM2). To purge the detectors with a quantity up to 2.5 l/m inert gas, the flow indicator (FI1) is used. Simultaneously, gas is removed from the system through the back pressure regulator (BPCV1). To have the stable content of fresh mixture, the R134a mass flow controller (FM1) operates the i-Butane controller (FM2). This means that FM1 flow controller is the master controller and FM2 flow controller is the slaves. These units are normally locally controlled. I-Butane flow is turned off if the R134a mixture is interrupted. The quantity of fresh mixture is monitored with the PC data acquisition/control system.

When the internal TOF chambers pressure, as measured by PIT4-PIT7 is more then 1.5" H20 above atmospheric, the gas control system will close the solenoid valves (SV2,SV3) in the fresh mixture supply line and open the vent line valve (SV9) allowing the mixture to vent directly to the atmosphere.. Also, the pressure indicating switch (PIS1) has a set-point of 1.50" H20

pressure and it can operate SV2, SV3, and SV9 through hardwired controls. Should the TOF cambers internal pressure reach 2" H20, the out going TOF chambers mixture will vent to the atmosphere through the safety bubbler. With this arrangement, the TOF chambers are protected from either flow controller malfunction, a rapid drop in atmospheric pressure and/or a failure of the back pressure regulator.

In the event of a rapid rise in atmospheric pressure, or effectively a fast drop in the TOF.W chambers internal pressure (up to 2.5" H2O/min), dual set point differential pressure transmitters (PIT4-PIT7) in the return manifold will trip as the pressure falls below 0.2" H2O causing an audible and visual alarm. When the pressure at PIT8 falls below atmospheric (0.05" H20 gage) a second set-point trips and the computer control system will stop compressor, shut off the flow of i-Butane, and flow inert gas by opening solenoid valve (SV1) to supply an additional 2.5 l/min of inert gas.

A pressure indicating switch (PIS1) with dual set points is installed in the return manifold. This switch is not connected to the computer control system but instead is hardwired to perform the same functions as computer in the event of a falling TOF.W chambers pressure. Thus the system is equipped with two separate means of preventing the TOF.W chambers from experiencing an external over or under pressure.

In the event of a power failure, the solenoid valves SV1, SV2 and SV9 will open, or remain open and SV3 will close, causing 2.5 l/min of inert gas to flow through the TOF chambers. This flow rate is adequate to assure that fluctuations in the atmospheric pressure will not result in the creation of over or negative pressure inside the TOF chambers.

The computer data acquisition /control system will measure the atmospheric pressure with a barometer (BP) to have the absolute pressure data.

6.f.3 Temperature Measurement

Two temperature transmitters (TT1, TT2) are used to measure the mixture temperature within the TOF chambers. The data of measured mixture temperature are logged for later use in data reduction.

6.f.4 Mixture Control

Along with automated valve control, the gas system's dedicated computer controlled data acquisition provides constant monitoring of the mixture composition by measuring the mass controllers output signals. I-Butane analyzer will be used periodically to check i-Butane content in the mixture. The mixture ratio is fixed by the Teledyne mass flow controllers (FM1, FM2) with the flammable gas "slaved" to R134a flow controllers. The stability of the flow controllers is sufficient to make variation in the mixture negligible.

6.f.5 Gas Sampling

The gas system is equipped with Oxygen, Moisture and i-Butane analyzers plumbed such that each section of the gas system can be selected separately for evaluation (through SV5, SV6, and SV7). All analyzer's data are read and archived by the computer data acquisition system and used to control the gas system.

6.f.6 Gas Purification

A gas dryer and purifier withdraws a portion (up to full amount) of the recirculating flow upstream of the pressure regulator (PCV1) and delivers the conditioned gas to the recirculating flow upstream of PCV1. This loop is used only as needed. The dryer is made from a stainless steel tube containing 1 lbs of molecular sieve (zeolite 13X) as the adsorbent. This amount permits the removal of about 0.4 lbs of water vapor to a level 2-3 ppm at room temperature. Filters are installed upstream and downstream of the adsorbent to prevent particles from entering to the mixture stream. A heating element is installed around the dryer which is then wrapped with fiber glass thermal insulation. The dryer is regenerated by heating it to 350-400C while purging with a mixture of Argon +5%H2. The purge gas enters at the top of the dryer and exits at the bottom carrying with it the water vapor. A temperature transmitter installed inside the dryer is connected to the temperature controller (TIC2) that supports the dryer temperature on the set-pointed level during regeneration. A moisture analyzer is used to measure the quantity of the water in the circuit before and after the dryer to determine when the adsorbent is saturated.

The purifier is similar to the dryer except that it is filled with a pure copper. The oxidization process takes place at 220 C that is supported with the temperature controller (TIC1). A heat exchanger (HE1) is used to reduce the mixture temperature coming into the dryer. This purifier is regenerated with the same purging gas as the dryer. Solenoid valve (SV8) installed at the inlet of the purification loop isolates the unit from the main circuit when it is not in use. If the inside pressure of purifier/dryer exceeds 1/3 PSI, the check valve (CV7) works as the safety valve and prevents the purifier/dryer from being damaged.

A 10 micron filter is installed after the purifier/dryer to prevent dust from passing into the main mixture supply line. A differential pressure transmitter (PT4) is used to determine when the filter needs to be replaced.

6.f.7 Computer Control and Data Acquisition

The gas system includes a computer driven data acquisition and control system. The controlling computer is a dedicated PC with Intel Pentium processor. It reads the data and operates the gas system through a National Instruments SCXI system. This computerized system is programmed to acquire the signals from the various temperature, pressure, flow and content measuring devices. It will issue warnings and/or take corrective action in the event that predetermined levels are exceeded. All acquired values can be selected and viewed on the terminal. The gas system can be monitored remotely through the internet though a secure host as well. The gas system alarms are sent to the Phenix Safety System and alerts the shift crews of any problems.

List of Fault Conditions		
Fault	Level	Action
1. PIT-8 purge(open SV1)	<0.05" H2O	Stop Compressor, gas
		Alarm(audible, flashing light)
2. PIT-8	<0.2" H2O	Alarm(audible, flashing light)
3. PIT-8	>1.50" H20	Alarm(audible, flashing light)
Close SV2, SV3 ; Open SV9		
		Alarm(audible, flashing light)
4. PT-1	<6PSI	Alarm(audible, flashing light)
5. PT-2	<6PSI	Alarm(audible, flashing light)
6. O2,H20	> 750 ppm,150ppm	Alarm(audible, flashing light)
7. O2, H2O	> 500 ppm, 100ppm	Alarm(flashing light)
8. I-Butane	> 7%	Alarm(audible, flashing light)
9. I-Butane	< 4%	Alarm(audible, flashing light)
10. FM1-2	>7%iC4H10	Stop iC4H10 supply.
		Alarm(audible, flashing light)
11. FM1-2	<4%iC4H10	Alarm(audible, flashing light)
12. PIT-1	<20" H2O	Alarm(audible, flashing light)
13. PT-4	>18" H2O	Alarm(audible, flashing light)
14. PT-8	> 4"H20	Alarm(audible, flashing light)

Table 3. List of fault conditions and alarms.

7. Production procedure, quality assurance.

The MRPC detectors will be produced, tested and assembled into the final gas boxes at Vanderbilt University and will be shipped to BNL ready for installation. The detectors will be built in a clean room and then tested with cosmic rays in a separate lab, such that the production and testing can proceed in parallel. We will use the general procedure that was already established during the prototype production. Improvements will be made in the steps that require manual control on positioning of different components. Appropriate jigs are currently being made, such that the production will proceed with grater accuracy and speed.

The total number of MRPC chambers to be installed is 128. We will build 150 (or more) detectors and the best performing detectors will be installed in PHENIX. The testing at Vanderbilt will include:

- **Performance test with cosmic rays.** Eight MRPC will be tested simultaneously in a stack with cosmic rays for 3 days. This time will be enough to collect a reasonable sample to perform streamer and rough timing studies. The percent of streamers at 14.5 KV will be measured. Less than 10% streamer contribution will be required. The timing signals from the MRPC will also be measured and monitored for any abnormal behavior.

- **Noise rate and leakage current measurements.** The noise rate will be measured with a random trigger and monitored for abnormal behavior. The leakage current will be monitored during the HV test.

- **1 week (or more) HV test in the final gas boxes.** The detectors will be assembled in the final gas boxes and a HV test will be performed for 1 week or more as time permits.

The gas boxes will be tested for leaks with a Freon leak detector before shipment.

The leak test will be repeated at BNL on the floor in 1008 before installation on carriage. HV will be applied at 1008 to all boxes before installation. Spare MRPCs will be available for replacement in the case that a detector was damaged in transport.

The pre-amp and FEM electronics will be delivered to BNL fully tested. Rice University assumes the responsibility for testing the pre-amps, while Nevis will test the FEMs.

All high voltage modules will be tested (and used during the test procedures) at Vanderbilt. The LV modules have already been used during RUN5 and require no additional testing.

8. Schedule and cost

The components for MRPC production are currently being ordered. We expect that initial deliveries that will allow the start of production will be made by the end of June 2005. The production of MRPCs will take 10 weeks (mid-September, 2005). The testing with cosmic rays will proceed in parallel. The production of the gas boxes will be finished by the end of August, 2005. The Feed-through boards are needed in order to close the gas volumes. These boards will be produced, tested and shipped from Rice University to Vanderbilt by Sept 1st, 2005. Assembly into the gas boxes and testing will take 2 weeks. The gas boxes will be shipped to BNL – Sept 30, 2005.

Tests on the floor at 1008 will be completed by Oct 15, 2005. Pre-amp electronics will be delivered to BNL on or before Oct 15th, 2005 fully tested. The preamp boards will be installed at 1008.

The detector will be installed on carriage in November, 2005.

FEM electronics will be delivered to BNL by Dec 15th, 2005.

The cost estimate is outlined in the table below.

	cost in k$	note
MRPC components, 20% contingency	85	
signal cables to patch panels	50	no quote
signal cables to FEM	50	no quote
mechanics	50	
HV system	60	available rough
pre-amps and F/T boards	100	estimate
FEMs , crates	246	
gas system	20	
total	661	

Table 4. Budget estimate.

9. Acknowledgement

10. References

[1] PHENIX Collaboration, K.Adcox et al., Phys. Rev. Lett. 88,022301,(2002).

[2] PHENIX Collaboration, K.Adcox et al.,Phys. Lett. B,561,19757(2003).
 STAR Collaboration, C.Adler et al., Phys. Rev. Lett. ,89,202301,(2002).

[3] PHENIX Collaboration, S.S. Adler et al.,Phys. Rev. Lett.,91, 072301 (2003)

[4] STAR Collaboration, C.Adler et al., Phys. Rev. Lett.,90,082302,(2003).

[5] STAR Collaboration, J.Adams et al.,submitted to Phys. Rev. Letters ,arXiv:nucl-ex/0306007.

[6] X.N.Wang and M.Gyulassy, Phys. Rev. Lett. 68, 1480, (1992); X.N. Wang, Phys Rev C58, 2321 (1998);
R.Baier et al., Phys. Lett. B345, 277 (1995).

[7] PHENIX Collaboration, S. S. Adler et al.,
Phys. Rev. Lett., 91, 072303 (2003) [arXiv:nucl-ex/0306021].

[8] STAR Collaboration, J.~Adams et al. , Phys. Rev. Lett., 91, 072304 (2003)

[9] PHOBOS Collaboration, B. B. Back et al. ,Phys. Rev. Lett. 91, 072302 (2003)

[10] BRAHMS Collaboration, I.~Arsene et al. ,Phys. Rev. Lett.,91, 072305 (2003)

[11] D. Kharzeev, E. Levin, L. McLerran, Phys. Lett. B 561,93,(2003).

[12] PHENIX Collaboration, S. S. Adler et al.,Phys. Rev. Lett.,91,172301,(2003)
[arXiv:nucl-ex/0305036].

[13] PHENIX Collaboration, S. S. Adler et al.,Phys. Rev. Lett., 91,182501,(2003)
[arXiv:nucl-ex/0305013].

[14] E.V.Shuryak,
Phys. Rev. C 66, 027902 (2002).[arXiv:nucl-th/0112042].

[15] D.Molnar and S.A.Voloshin, arXiv:nucl-th/0302014.

[16] STAR Collaboration, J. Adams et al., submitted to Phys. Rev. Lett. Sept. 16, 2003. [nucl-ex/0309012]
 [17] Proposal for a Large Area Time of Flight System for STAR, http://wjllope.rice.edu/~TOF/
[18] CERN/LHCC 2002-016 Addendum to ALICE TDR 8, 24 April 2002